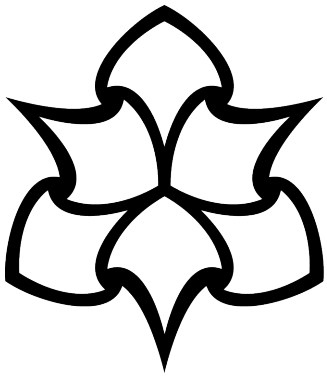

Muscle moment arm analyses applied to vertebrate paleontology: a case study using *Stegosaurus stenops* Marsh, 1887

CHARLOTTE A. BRASSEY,[1,†,*] SUSANNAH C. R. MAIDMENT,[2,3] and PAUL M. BARRETT[4]

[†]Current Address: School of Science and the Environment, Manchester Metropolitan University, Chester Street, Manchester, M1 5GD, United Kingdom, c.brassey@mmu.ac.uk;

[1]School of Earth and Environmental Sciences, University of Manchester, Manchester, M13 9PL, United Kingdom;

[2]School of Environment and Technology, University of Brighton, Lewes Road, Brighton, BN2 4GJ, United Kingdom, s.maidment@brighton.ac.uk;

[3]Department of Earth Science and Engineering, South Kensington Campus, Imperial College, London SW7 2AZ, United Kingdom;

[4]Department of Earth Sciences, The Natural History Museum, Cromwell Road, London SW7 5DB, United Kingdom, p.barrett@nhm.ac.uk

*Corresponding author

ABSTRACT—The moment arm of a muscle defines its leverage around a given joint. In a clinical setting, the quantification of muscle moment arms is an important means of establishing the 'healthy' functioning of a muscle and in identifying and treating musculoskeletal abnormalities. Elsewhere in modern animal taxa, moment arm studies aim to illuminate adaptions of the musculoskeletal system towards particular locomotor or feeding behaviors. In the absence of kinematic data, paleontologists have likewise relied upon estimated muscle moment arms as a means of reconstructing musculoskeletal function and biomechanical performance in fossil species. With the application of 'virtual paleontological' techniques, it is possible to generate increasingly detailed musculoskeletal models of extinct taxa. However, the steps taken to derive such models of complex systems are seldom reported in detail. Here we present a case study for calculating three-dimensional muscle moment arms using *Stegosaurus stenops* Marsh, 1887 to highlight both the potential and the limitations of this approach in vertebrate paleontology. We find the technique to be mostly insensitive to choices in muscle modeling parameters (particularly relative to other sources of uncertainty in paleontological studies), although exceptions do exist. Of more concern is the current lack of consensus on what functional signals, if any, are contained within moment arm data derived from extant species. Until a correlation between muscle moment arm and function can be broadly identified across a range of modern taxa, the interpretation of moment arms calculated for extinct taxa should be approached with caution.

INTRODUCTION

Biomechanics is the application of mechanical principles to biological systems. An understanding of how mechanical principles act to facilitate or constrain biological form is essential for our understanding of adaptation and the causal link between phenotype and evolutionary success (Alexander, 2003; Taylor and Thomas, 2014). At the level of the individual, the fundamental processes of locomotion, feeding, breathing, and reproduction are strongly dictated by the geometric arrangement of muscle and bone. More broadly, studies of predation, competitive exclusion, adaptive radiation, and convergent evolution may all be considered in the light of the musculoskeletal system.

Here, we focus on one particular aspect of functional anatomy, muscle moment arms, or the leverage of muscles around a joint. As a geometric property, moment arms can be straightforward to calculate, and have therefore been widely applied to fossil taxa to elucidate evolutionary trends in biomechanical performance within and between extinct lineages, and higher-level biomechanical parameters such as active muscle volume and estimated energy expenditure. With the recent growth in 'virtual paleontology' (Sutton et al., 2014), increasingly advanced modeling techniques are now employed to estimate muscle moment arms. Using a new 3D digital reconstruction of *Stegosaurus stenops* (Brassey et al., 2015) as a worked example, we describe in detail the steps taken when calculating muscle moment arms in fossil taxa. In particular, we highlight the relative sensitivity/insensitivity of this approach to modeling parameters. Additionally, we discuss what functional signals, if any, are present in the muscle moment arms of extant taxa, and the degree to which these signals may be discernable in fossil taxa.

67

68 **Muscle Moment Arms in Extant Taxa**

69 In biomechanics, musculoskeletal function is strongly dictated by the
70 geometry of the muscle-tendon units of the body, and the most basic descriptor of
71 muscle geometry is muscle moment arm. Torque (or moment) is the tendency for an
72 applied force to rotate an object around an axis, and is calculated as the cross product
73 of force and the lever-arm (herein 'moment arm') of the force system (Gregory,
74 2006). The moment arm is defined as the perpendicular distance from said axis to the
75 line of action of the force. In the context of biomechanics, a muscle moment arm can
76 be thought of as the leverage of a given muscle-tendon unit around a joint and as a
77 means of transforming muscle force into joint rotation. As such, moment arms are
78 crucial for understanding how muscles produce limb movement. In this simplified
79 lever system, larger moment arms produce larger joint moments as:

80

81 $$M_{joint} = MA \times F_{mus} \quad (1)$$

82

83 where M_{joint} is the joint moment, MA is the moment arm, and F_{mus} is the muscle force.
84 However, larger moment arms are also associated with a decrease in muscle
85 contraction velocity as:

86

87 $$\omega = \tan^{-1}(\Delta L_{mus}/\mathrm{MA})/t \quad (2)$$

88

89 where ω is the angular velocity of the joint, ΔL_{mus} is the change in the length of the
90 muscle, and t is time (Channon et al., 2010). Muscle moment arms may therefore

91 distinguish between limbs optimized for high rotational velocity versus those
92 optimized for high torque (Stern, 1974; but see below for confounding factors).
93 Within human clinical and sports sciences, the quantification of 'healthy'
94 muscle moment arms is essential for the treatment of movement abnormalities and in
95 the planning of orthopedic surgeries (Arnold et al., 2000). Therefore considerable
96 effort has been invested in developing techniques for reliably estimating muscle
97 moment arms. For cadaveric material, muscle moment arm can be calculated
98 according to the classic 'geometric' definition (the shortest perpendicular distance
99 from the joint center of rotation to the muscle-tendon unit's line of action) using an
100 idealized origin-insertion model, assuming each muscle is represented as a straight
101 line between origin and insertion (Karlsson and Peterson, 1992; Hughes et al., 1998;
102 see Fig. 1).
103 However, moment arm often varies with joint angle (An et al., 1984), and
104 hence muscle dynamics vary throughout the gait cycle (Williams et al., 2008).
105 Consequently, a more informative metric is the relationship between joint angle and
106 instantaneous muscle moment arm. The tendon-travel method (Spoor and van
107 Leeuwen, 1992; Otis et al., 1994) plots joint angle against tendon displacement and
108 fits linear or second/third order polynomial models to the relationship. The equations
109 can then be differentiated to give either a constant value for moment arm (as in the
110 case of linear regression) or the relationship between joint angle and moment arm (in
111 the case of polynomial equations). The tendon-travel method benefits from
112 minimizing the uncertainty associated with locating the joint center and has been
113 applied extensively to both human and non-human modern taxa (Favre et al., 2008;
114 Channon et al., 2010; Crook et al., 2010; Astley and Roberts, 2012). However,
115 concerns have been raised regarding the application of tendon-travel to the calculation

of moment arms. Sustaita et al. (2015) found considerable disagreement between moment arms calculated using the 'geometric' definition and those calculated via tendon-travel, most likely due to dynamic changes in the travel path of tendons during phalangeal joint excursion causing increased tendon travel without a concomitant increase in a given in-lever. Additionally, Hutchinson et al. (2014) highlighted the issue of kinematic 'cross-talk', in which the joint coordinate system is misaligned with the axis about which movement is assumed to occur (for example, the flexion-extension axis may deviate from the mediolateral anatomical direction: Piazza and Cavanagh, 2000). Thus, physical manipulation of the joint within one plane of movement will inevitably produce some motion about the others, introducing additional error into tendon-travel estimates.

Traditionally applied, both methods for estimating moment arms assume the joint to be operating solely within the plane of movement under investigation (i.e., ignoring the 'cross-talk' described above), and involve labor-intensive dissection. Increasingly, however, 3D medical imaging techniques, such as computed tomography (CT), magnetic resonance imaging (MRI), and ultrasound, are being employed to carry out in-vivo subject-specific quantification of muscle moment arms (Sammarco et al., 1973; Kumar, 1988; Juul-Kristensen et al., 2000; Maganaris, 2004), either for the purpose of surgical planning and clinical decision-making or for ex-vivo quantification based on cadaveric material. These approaches avoid invasive surgeries and allow joint movement to be quantified in 3D. However, calculating muscle moment arms for the wide variety of limb postures assumed during habitual locomotion requires extensive imaging of the patient. Therefore a combination of patient-specific 3D imaging and generic computer-based musculoskeletal modeling

has become common practice in clinical biomechanics (Arnold et al., 2000 and references therein).

Muscle Moment Arms Applied to the Fossil Record

Within the disciplines of paleontology and physical anthropology, bone morphology is often the only source of information upon which to base reconstructions of the behavior and phylogenetic relationships of extinct species. Other information on bone material properties (elastic moduli, density) and muscle architecture (fiber length, pennation angle) are either lost entirely or preserved only under exceptional conditions (McNamara et al., 2010). When required for biomechanical modeling approaches, such as finite element analysis (FEA) or multibody dynamic analysis (MBDA), these properties must therefore be estimated with reference to the extant phylogenetic bracket (EPB: Witmer, 1995a) or explicitly excluded from the analysis.

Although soft tissues are rarely preserved in the fossil record, musculoskeletal reconstructions of extinct taxa are frequently attempted (e.g., fish: Anderson and Westneat, 2009; early tetrapods: Neenan et al., 2014; amphibians: Witzmann and Schoch, 2013; dinosaurs: Maidment and Barrett, 2011, 2012; pterosaurs: Costa et al., 2013; mammals: Gill et al., 2014; birds: Tambussi et al., 2012; hominins: Nagano et al., 2005; D'Anastasio et al., 2013). Furthermore, the qualitative discussion of muscle moment arms is a long-established practice in vertebrate paleontology (Morton, 1924; Simpson and Elftman, 1928), and the calculation of muscle moment arms has been applied to the fossil record to address biomechanical questions at several levels:

1. The functioning of individual muscle-tendon units. For example, determining the function of a particular muscle (i.e., flexor vs. extensor) around a given joint in an individual (e.g., Bates et al., 2012a).

2. The functioning of musculoskeletal groups. For example, using the sum of muscle moment arms around a joint to infer limb pose in an individual (e.g., Hutchinson et al., 2005).

3. The functioning of muscle-tendon units, or musculoskeletal groups, across multiple individuals. For example, using muscle moment arms to infer changes in locomotor ability, feeding or other behaviors within a lineage (e.g., Bargo, 2001).

In the absence of soft tissues, muscle moment arms may be calculated from dry skeletal/fossil remains on the basis of estimated muscle attachment sites, simple 2D trigonometry, and/or more complex 3D computer models. Early studies tended to follow an idealized 2D origin-insertion method (e.g., DeMar and Barghusen, 1972; McHenry, 1975; Emerson and Radinsky, 1980) in which each muscle is simplified to one line of action, and a single value for a moment arm is calculated geometrically on the basis of skeletal landmarks identifying joint centers and muscle insertions (see Fig. 1). However, following the development of computer-based musculoskeletal modeling within the clinical sciences, paleontologists have adopted this technique to generate detailed 3D models of fossil myology including complex joints, muscle geometry, and travel paths for the purpose of moment arm estimation (e.g., Hutchinson et al., 2005; Chapman et al., 2010; Bates and Schachner, 2011; Bates et al., 2012a, b; Maidment et al., 2014a; Costa et al., 2013). Both approaches have merit, and both are still commonly applied to calculate the muscle moment arms of extinct taxa.

187 Van Der Helm and Veenbaas (1991) identified two phases in assessing the
188 mechanical behavior of a system: 1) deriving an adequate model of the system and; 2)
189 using the model to calculate forces, stresses, and motions. In the case of the
190 musculoskeletal system, once a model has been created, the calculation of muscle
191 moment arms, muscle force, joint torque, etc., is relatively straightforward and has the
192 potential to generate a vast quantity of data very quickly. In some cases, however,
193 only the results of the analyses are discussed in detail, whereas the steps taken to
194 derive a simplified model of a fossil from such a complex system may be poorly
195 described or absent entirely.
196 Elsewhere, considered reviews of paleontological FEA have highlighted the
197 sensitivity of model results to input parameters and cautioned against their over-
198 interpretation (Rayfield, 2007; Bright, 2014), reflecting a growing concern within the
199 field over the exponential growth in the number of fossil biomechanics studies with
200 comparatively little validation on extant taxa (Anderson et al., 2011; Brassey, in
201 press). Here we contribute to this discussion by reviewing the procedure for
202 calculating muscle moment arms using 3D musculoskeletal models of fossil species,
203 highlighting the steps that involve user subjectivity and potential sources of
204 uncertainty in model parameters. Whilst the growth in graphics-based computational
205 models has made it possible to create increasingly complex and arguably more
206 'realistic' biomechanical models of fossil taxa, this has been at a cost. Much of the
207 literature surrounding musculoskeletal models of fossil species is an impenetrable
208 'black-box' to non-specialists (Anderson et al., 2011) as methodologies are often
209 sparse in detail or relegated to supplementary materials (although see Domalain et al.,
210 2016; Lautenschlager, 2016). Furthermore, the sensitivity of model results to input

parameters are not always fully explored (although see Hutchinson et al. [2005] and Bates et al. [2012a] for sensitivity analyses on fossil muscle reconstructions).

Here we present a workflow for the generation of a musculoskeletal model of a specific fossil individual and the subsequent calculation of muscle moment arms. We aim to improve transparency with regard to model creation, whilst emphasizing the potential utility of this approach and drawing attention to its limitations. Previous studies have addressed these issues in the context of clinical human anatomy (Hicks et al., 2014 and references therein), but we highlight additional issues that are solely the concern of those working on fossil material. Furthermore, we consider which functional signals (if any) are discernable within the muscle moment arm data of extant taxa, and therefore what we might reasonably expect to find from an equivalent paleontological study.

The capacity of a given muscle to generate torque around a joint is a function of both its force-generating capability (as defined by physiological cross-sectional area) and its moment arm. Multibody dynamic analyses employing forward- or inverse-dynamic simulations of locomotion (Sellers and Manning, 2007; Sellers et al., 2009, 2013), biting (Bates and Falkingham, 2012; Lautenschlager et al., 2016) and head and neck movements (Snively et al., 2013) in fossil species are also reliant upon estimates of both muscle architecture and muscle moment arms. The following discussion is therefore highly relevant to those creating musculoskeletal models for the purpose of MBDA and FEA on extinct species.

MODEL CONSTRUCTION

The specimen used as an example herein is a sub-adult individual of the ornithischian dinosaur *Stegosaurus stenops* Marsh, 1887 (NHMUK [Natural History Museum, London, U.K.] PV R36730), collected from the Upper Jurassic Morrison Formation of Wyoming, U.S.A. This specimen is the most complete *Stegosaurus* found to date, with over 80% of the body represented (Brassey et al., 2015; Maidment et al., 2015). The specimen was digitized as disarticulated elements using photogrammetric protocols described elsewhere (Falkingham, 2012; Mallison and Wings, 2014) and the freely available photogrammetry software 'VisualSFM' (http://ccwu.me/vsfm) and 'Meshlab' (http://meshlab.sourceforge.net) and the reconstructed articulated skeleton was posed in 3DsMax (www.autodesk.com/3dsmax) (see Fig. 2). Details regarding the extent of missing/repaired elements and degree of taphonomic damage are reported elsewhere (Maidment et al., 2015). Likewise, the procedure for rearticulating the digital model is documented in Brassey et al. (2015).

Muscle moment arm analysis was carried out in 'Gaitsym' (http://www.animalsimulation.org; Sellers and Manning, 2007). Whilst we take a 3D graphics-based computational approach to calculating moment arms of the appendicular skeleton, much of our discussion is also applicable to the classic 2D origin-insertion method frequently employed by paleontologists and to musculoskeletal reconstructions of the skull.

The procedure for model creation is described in detail below. Briefly, muscles were reconstructed on the basis of stegosaurian limb myology, as reconstructed by Maidment and Barrett (2012), including 13 muscles in the forelimb and 19 in the hind limb. In addition, pairs of antagonistic puppet-string 'driver' muscles were attached for the purpose of driving the limbs from maximal theoretical

flexion to maximum theoretical extension (see Fig. 2 and 'Joint Ranges of Motion', below, for more detail). Alternatively, pre-existing muscles within the model can be used for this purpose, assuming the geometry of the muscle is such that the maximum flexion/extension can be achieved when the muscle is activated. Whichever mechanism is used to drive the limb through flexion-extension (either by the puppet-string muscles, or by firing off the pre-existing muscles intrinsic to the model), joint limits are predetermined (see below) and will remain the same, as will the resulting moment arms.

Moment arms were calculated according to the classic geometric definition (shortest perpendicular distance from joint center to muscle line of action) as opposed to the tendon travel method, although both will result in the same answer using the 3D modeling approach presented herein. As the model comprised several bi-articular muscles (muscles that travel across two joints), joints in the limb other than the one under investigation were locked in all planes of movement during the analysis, as is common practice in paleontology and modern cadaveric experiments (Channon et al., 2010). Pairs of driver muscles were activated in sequence (each activation lasting 0.5 seconds) to drive the limb segment through its full range of motion from its original neutral posture whilst instantaneous moment arms were calculated for every muscle at a default interval of 0.0001 seconds. Joint angle and moment arms were exported to 'R' (R Core Team, 2016) and plotted using a cubic smoothing spline (smooth.spline function within the 'stats' package).

Articulation of the Skeleton

Every mechanical model begins with at least two rigid bodies (in this case, bones) connected by a kinematic constraint (in this case, a joint). When generating a

musculoskeletal model of an extant individual, skeletal geometry is often derived from a CT or MRI scan of the intact body and the articulation of the skeleton is therefore relatively well constrained. In the case of fossil taxa, however, the skeleton may be digitized as disarticulated elements (as in the case of *Stegosaurus* presented here) or as a museum-mounted specimen (Maidment et al., 2014). In either scenario, the absence of associated soft tissues requires subjective decisions to be made regarding the rearticulation of the skeleton.

Although the preservation of calcified cartilage in fossil long bones has been widely reported (Holliday et al., 2010 and references therein), the non-ossified epiphyseal joint cartilage (chondroepiphysis) that would have capped the ends of bones is rarely fossilized (Chinsamy-Turan, 2005). In extant archosaurs, removal of the chondroepiphysis accounts for a 5–9% decrease in long bone length in the limbs of *Alligator mississippiensis* and 0–10% in a range of modern birds (Holliday et al., 2010). Previous studies of fossil muscle moment arms have attempted to correct for this missing cartilage. In a study on the hind limbs of *Tyrannosaurus rex*, Hutchinson et al. (2005) added 7.5% to the length of the femur, 5% to that the tibia, and 10% to metatarsus length on the basis of an undescribed set of cartilage measurements from extant taxa. In other studies limb bones are clearly spaced apart, yet no specific reference is made to the size of spacing, nor how this value was calculated (e.g., Bates et al., 2012a, b).

Failure to account for missing articular cartilage has the effect of shortening the effective segment length and bringing muscle origin and insertion points closer together. As an example, Figure 3 illustrates the effect of incorporating articular cartilage on moment arm values for the M. iliofibularis (IFB) measured around the knee during knee flexion. IFB was modelled as travelling in a straight path from

310 origin to insertion without passing through via points or around cylinders (see Muscle
311 Paths, below). For a discussion of the process of estimating joint center locations, see
312 Joint Centers, below. The effect of missing articular cartilage on calculated moment
313 arms varies with joint angle (Fig. 3) with the discrepancy between models with and
314 without cartilage increasing with knee flexion. When accounting for an additional
315 (worst-case scenario) 10% of long bone length as cartilage (Fig. 3C), the maximum
316 value calculated for IFB moment arm is 26% greater than when cartilage is ignored.
317 However, if the joint center is shifted distally to maintain an equal distance between
318 muscle insertion and center of rotation when adding cartilage (Fig. 3D), this
319 discrepancy is considerably reduced. In modern taxa, the extent to which joint center
320 locations differ between those calculated in-vivo, versus those based on dry articular
321 surfaces missing cartilage, is unknown (see later section 'Joint Centers').
322 Given that high variability has been documented in long bone cartilage
323 thickness among extant birds (within Galliformes, cartilage accounts for 10% of
324 femoral length in *Gallus gallus* and 1% in *Coturnix japonica*: Holliday et al., 2010) it
325 is reasonable to predict that such disparity might also have characterized extinct
326 clades. When generating muscle moment arm data across a comparative sample of
327 fossil taxa, for example, the dinosaurian clades Ornithischia (Maidment et al., 2014a)
328 or Allosauroidea (Bates et al., 2012b), it is prudent to consider that interspecific
329 variability in cartilage thickness will overlie any hypothesized functional signal in
330 muscle moment arms, and may affect the interpretation of the dataset. In extant
331 mammals, a significant negative allometric relationship exists between body mass and
332 femoral condyle cartilage thickness (Malda et al., 2013). A similar pattern has also
333 been identified in ontogenetic samples of *Alligator* and *Numida*, in which smaller
334 individuals possess a relatively greater thickness of chondroepiphysis to total bone

length (Bonnan et al., 2010). Should this relationship prove consistent across modern birds or reptiles, it would prove useful in constraining hind limb joint spacing in comparative samples of fossil archosaur taxa.

Likewise, the loss of intervertebral fibrocartilagenous disks or synovial capsules from between adjacent vertebrae in extinct taxa has the effect of shortening the length of the reconstructed vertebral column. This effect has previously been discussed in the context of estimated neck flexibility and range of motion (Mallison, 2010a; Cobley et al., 2013; Taylor and Wedel, 2013) and as a potential source of uncertainty in volumetric mass estimates (Brassey et al., 2015). Additionally, for muscles originating from the tail (e.g., M. caudofemoralis longus in archosaurs) or thorax (e.g., M. latissimus dorsi and M. trapezius in tetrapods), the incorporation of additional spacing to account for intervertebral soft tissues will also impact calculated muscle moment arms in a similar manner to epiphyseal cartilage, as discussed above. Furthermore, placement of the scapula relative to the ribcage has a knock-on effect on the location of the shoulder joint relative to the thorax. Whilst mounted skeletons are often characterized by the scapula immediately overlying the ribs, the volume of soft tissue separating the skeletal elements has not been quantified in extant taxa.

In addition to joint spacing, the joint morphology of extinct taxa can be altered, both due to the removal of cartilage and other soft tissues though the process of fossilization (Bonnan et al., 2010), and due to subsequent taphonomic deformation and weathering. This can increase uncertainty with regards to the orientation and positioning of skeletal elements, and further hamper efforts during rearticulation. In the case of *Stegosaurus* (NHMUK PV R36730), for example, the degree of mediolateral flaring of the pubis and ischium is open to interpretation.

In ornithischian dinosaurs, the prepubis is an anterior extension of the pubis arising from its proximal margin and extending anterior to the acetabulum. This process acts as an origin for the M. ambiens (AMB), which subsequently inserts onto the cnemial crest of the tibia (Maidment and Barrett, 2011). When reconstructing the *Stegosaurus* model, the pubis and ischium were rearticulated with the ventral surface of the ilium to form the borders of an open acetabulum using the orientations of their articular surfaces as a guide. However, the angles at which the paired pubes and ischia extend with respect to the midline are uncertain. Whilst the paired pubes must be in contact distally, the contact between the iliac articulation of the pubis and the pubic peduncle of the ilium is less well constrained by osteology. Figure 4 illustrates the effect of varying the angle of the pubis relative to the midline on AMB flexion-extension (FlexExt), abduction-adduction (AbdAdd), and long-axis rotation (LAR) moment arms calculated at the hip during hip flexion-extension. The pubis was modeled in two orientations: a) with the long axes of the pubes aligned parallel to the iliac blades (Fig. 4A), which are themselves extremely flared in the mediolateral direction, with their distal ends meeting at a ventral midline symphysis; and b) with the long axes of the pubes rotated medially from this initial position, with distal ends meeting in a symphysis but with less extreme flaring (Fig. 4B).

Predictably, rotating the pubis medially does not impact upon the flexion-extension moment arm of AMB, and the functioning of the muscle remains consistent as a flexor. Likewise, AbdAdd moment arms for both model configurations suggest AMB functions as a hip abductor as the origin as path of the muscle remains lateral to the hip joint throughout the range of motion. When the pubis is rotated medially, average AbdAdd moment arm does decrease from 0.23 to 0.14 m, however, due to the muscle path shifting closer to the joint center. Interestingly LAR moment arms in the

384 flared pubis model suggest a lateral rotation function at values of hip flexion between
385 35–60° (Fig. 4A), whereas AMB acts as a medial rotator throughout most of the
386 range of motion in the medial pubis model, switching to lateral rotation only at very
387 high values of flexion (>50°) and representing a small change in predicted muscle
388 function between the two models.

389 Uncertainty with regards to skeletal articulation therefore has the potential to
390 affect not only the magnitude of calculated muscle moment arms, but also the inferred
391 function of the muscle unit itself. This highlights the importance of having a strong
392 grounding in both the osteology and myology of the study taxa and in conducting
393 sensitivity analyses, not only to quantify uncertainty in muscle attachment sites, as has
394 previously been the case (Hutchinson et al., 2005; Bates et al., 2012a), but also to
395 investigate the effects of uncertainty in skeletal articulation.

396 Finally, the neutral stance in which the model is posed must be clearly stated
397 in order to facilitate comparisons between species and across studies. For some
398 muscles, moment arm values calculated with respect to a given joint axis are highly
399 sensitive to the joint angle about one or both of the other axes (O'Neill et al., 2013),
400 as highlighted by the issue of 'cross talk' when estimating extant moment arms via the
401 tendon-travel method (Hutchinson et al., 2014; see Introduction). For the estimation
402 of hind limb muscle moment arms in dinosaurs, a standard neutral hip posture of 0°
403 extension, 10° abduction, and 0° long axis rotation has been broadly agreed upon
404 (Hutchinson et al., 2005; Bates and Schachner, 2011; Bates et al., 2012a; Maidment et
405 al., 2014a), a convention that we follow herein. Comparatively little work has been
406 carried out on the moment arms of forelimb muscles in extinct taxa using 3D
407 musculoskeletal models (although geometric 'dry-bone' analyses do exist: Fujiwara
408 and Hutchinson, 2012; Martín-Serra et al., 2014). We therefore assume a neutral

409 shoulder posture of 30° retraction, 10° abduction, and 0° long axis rotation, following
410 this earlier work.
411 Undoubtedly, the selection of a 'neutral posture' does introduce a degree of
412 uncertainty and places unnecessary emphasis on reconstructing the standing posture
413 of individual taxa. When undertaking a comparison between several species of
414 differing bone morphology, the degree of osteological rotation around the long axis of
415 the bone, or extent of valgus, may vary. In such an instance, identifying an
416 'equivalent' starting point for a moment arm analysis may prove problematic. An
417 alternative way forward may be to follow the protocol used in biplanar X-ray imaging
418 studies (M. F. Bonnan, pers. comm., January 2017), in which the bones may be posed
419 in a flat plane or a folded position (Bonnan et al., 2016). Such reference postures
420 might be anatomically unfeasible, but are more easily replicated across a wide range
421 of taxa of diverse morphology and would provide a more consistent starting point for
422 comparative muscle moment arm studies.
423
424 **Joint Ranges of Motion**
425 Muscle moment arm can change as a function of joint angle (An et al., 1984)
426 and it is common practice to report moment arm values calculated as a limb is moved
427 through its full range of motion (ROM) in a particular plane. In Figure 4, for example,
428 the hip joint is moved from full flexion (-60°) to full extension (60°), assuming a
429 neutral posture of 0° in which the femur is held perpendicular to the ground in the
430 sagittal plane. It is important to emphasize that the selection of the joint ROM is
431 entirely under the control of the user. That is, whilst it is possible to calculate a value
432 for muscle moment arm for absolutely any joint angle (including angles at which the

433 limb would be entirely disarticulated), it is at the discretion of the user to constrain the
434 ROM to within probable biomechanical limits.
435 For example, Maidment et al. (2014a) compared hind limb muscle moment
436 arms calculated for a diverse sample of ornithischian dinosaurs across a hip flexion-
437 extension ROM of -60° to 60°. Whilst this approach of comparing species across a
438 fixed ROM simplifies comparisons, it does raise a teleological issue. The
439 biomechanical feasibility of each individual achieving such a ROM in-vivo is not
440 taken into account, and on the basis of osteological and myological reconstructions it
441 is considered highly unlikely that some species (including this specimen of
442 *Stegosaurus*) could have attained the lower-most values for hip flexion (see Fig. 5).
443 The value of plotting muscle moment arms calculated at unrealistic joint angles is
444 therefore questionable.
445 An alternative approach is to investigate feasible joint ROM on a specimen-
446 by-specimen basis, either through physical rearticulation of the skeleton or casts
447 thereof (Johnson and Ostrom, 1995; Senter and Robins, 2005; Taylor and Senter,
448 2010) or through manipulation of 3D digital models (Mallison, 2010a, b; Pierce et al.,
449 2012). However previous studies have found ROM at the joints to be strongly affected
450 by the presence/absence of soft tissues and cartilage around limb (Hutson and Hutson,
451 2012) and intervertebral joints (Taylor and Wedel, 2013; Cobley et al., 2013), and
452 accounting for the removal of extrinsic (integument, muscles, capsular ligaments) and
453 intrinsic (cartilage) soft tissues from the fossil skeleton is not straightforward. Within
454 the shoulder and elbow of *Alligator*, for example, the removal of extrinsic soft tissues
455 acts to increase ROM, whilst subsequent removal of articular cartilage acts to
456 decrease ROM, resulting in a counter-intuitive net decrease in ROM from an intact to
457 entirely skeletonized limb (Hutson and Hutson, 2012, 2013). In contrast, within the

458 neck of the ostrich, removal of both extrinsic and intrinsic soft tissues acts to increase
459 ROM (Cobley et al., 2013). A growing body of work is quantifying joint ROM both
460 in non-human mammals (Ren et al., 2008; Bonnan et al., 2016) and within the context
461 of the dinosaur EPB, although the total number of studies remains limited. In light of
462 this paucity of modern data, the conservative approach of Maidment et al. (2014a),
463 where all taxa are modelled with the same broad ROM, may be preferable. However,
464 the requirement for anatomically realistic ROM data remains an issue for MBDA of
465 locomotion, feeding, etc.

466 Furthermore, assessments of possible joint ROM tend to focus solely on bone-
467 to-bone contact within the fossil limb, such as joint impingement and dislocation. For
468 example, moment arm papers dealing with hind limb muscles in extinct taxa often
469 model the bones of the pelvis and hind limb only (Hutchinson et al., 2005; Bates et
470 al., 2012a, b; Maidment et al., 2014a, b). Potential collisions with the head, arms, and
471 torso are ignored. Yet, as illustrated in Figure 5, the positioning of the ribcage can act
472 as a further constraint on joint ROM, as the extent of hip flexion is limited by the
473 potential for the femur to collide with the posterior dorsal ribs (assuming 10°
474 abduction and zero long axis rotation). However, this approach is considerably more
475 time consuming (as digital models of the thoracic vertebrae and dorsal ribs are also
476 required) and places further onus upon accurate rearticulation of the trunk, which is
477 itself subject to various assumptions (e.g., the potential range of movement between
478 the rib and its vertebral articulations, the exact geometry of the articulations, and the
479 effects on these of missing soft tissues). In our *Stegosaurus* model, for example, the
480 characteristic triangular ribcage present in the skeletal mounts of the American
481 Museum of Natural History and Senckenberg Museum stegosaurs is reconstructed by
482 sweeping the distal ends of the ribs anteriorly (Fig. 5). Yet ribs are frequently

damaged, taphonomically deformed (e.g., Maidment et al., 2015), or absent entirely, and the extent to which this represents an accurate skeletal rearticulation is unclear. Whilst the incorporation of additional body parts, such as the tail or torso, into a musculoskeletal model may further constrain limb ROM, this must be balanced against a concurrent increase in uncertainty regarding model articulation and also the concomitant reduction in analytical sample size, which becomes limited perforce to those specimens that are relatively complete. On the rare occasions when trackways can be assigned confidently to fossil taxa, their gauge, stride length, and other track features may also inform potential posture and limb range of motion (e.g., Alexander, 1989; Henderson, 2006; Hatala et al., 2016; but see Falkingham, 2014).

Muscle Definitions

Muscle Anatomy—Following the articulation of rigid bodies, the next stage in building our biomechanical model involves reconstruction of the overlying musculature. As highlighted above, it is possible to output moment arm values for an array of nonsensical musculoskeletal arrangements, but we emphasize and advocate the importance of grounding fossil biomechanical studies within a comprehensive understanding of the anatomy of the study taxa. In the case of fossil myologies, accurate reconstructions require the assimilation of two sources of information (Fox, 1964): 1) evidence of muscle attachment sites on bone surfaces, including scarring, ridges, trochanters, and fossae; and 2) phylogenetic inference of muscle presence/absence based of the anatomy of closely related extant taxa (Witmer, 1995a).

The use of osteological correlates in soft tissue reconstruction is well established in vertebrate paleontology. Muscle scarring can indicate the location and,

508 to a limited extent, the size of a muscle attachment, and has been applied to broad
509 interspecific samples of taxa to trace the evolution of cranial (Witmer, 1995b;
510 Holliday, 2009) and postcranial musculature (Hutchinson, 2001a, b; Maidment and
511 Barrett, 2012). Muscles inserting via tendons or aponeuroses tend to leave more
512 distinct scars than those inserting via fleshy attachments (Bryant and Seymour, 1990),
513 yet those without well-developed scars may still be reconstructed with a reasonable
514 level of confidence (Hutchinson and Carrano, 2002) particularly when placed within a
515 phylogenetic context (see below). The correspondence between the location of
516 attaching muscles and resulting scars has been validated in extant taxa, in both the
517 skull (Hieronymus, 2006) and postcrania (Hutchinson, 2002; Meers, 2003), although
518 recent research has cautioned against the interpretation of scar morphology as
519 representative of original muscle size and/or action (Zumwalt, 2006).
520 Application of the EPB approach can further constrain soft tissue inferences
521 (Bryant and Russell, 1992; Witmer, 1995a). At its most straightforward, the EPB
522 places fossil taxa within the phylogenetic context of their closest related extant taxa,
523 with any condition present in both extant taxa being inferred as present in their last
524 common ancestor and in all of its descendants. For the purpose of estimating moment
525 arms, the EPB also has the advantage of permitting the reconstruction of muscles that
526 lack distinct attachment scarring. Furthermore, application of the EPB to soft tissue
527 restoration involves a 'hierarchy of inferences' and reconstructions are assigned to
528 levels I, II, or III depending upon the degree of speculation involved (Witmer, 1995a).
529 This categorization therefore allows the degree of uncertainty in reconstructed
530 myology to be recorded and communicated. Depending on the taxa of interest,
531 however, the EPB can be relatively broad and encompass modern taxa that may be
532 too functionally divergent from the fossil species to provide a basis for useful

comparisons (for example, extant amphibious crocodiles form part of the EPB for extinct flying pterosaurs). This highlights the importance of grounding fossil muscle reconstructions in a detailed understanding of the complexity and variability that characterizes modern taxa, and the value of traditional anatomical descriptions as a necessary precursor to further functional analyses.

To Clump or To Split?—Every biomechanical model represents a trade-off between realism, precision, and generality, and in the case of musculoskeletal models, this trade-off is particularly evident in myological reconstructions. The detail required of a musculoskeletal model is a function of the question under investigation. In some instances, all muscles acting around a particular joint are reconstructed in order that the sum total moment arm may be estimated and limb posture inferred (Hutchinson et al., 2005; Payne et al., 2006; Maidment et al., 2014a). In other instances, when the question under consideration seeks to address an aspect of biomechanical performance across a large comparative sample, only 'major muscles' may be reconstructed. Biomechanical models of the masticatory system of fossil mammals, for example, often include only the major jaw adductors, the M. temporalis and M. masseter, in moment arm calculations (Iuliis et al., 2001; Bargo, 2001; Vizcaíno and Iuliis, 2003; Cassini and Vizcaíno, 2012). In such instances, the decision regarding which muscles to include is often made on the basis of reconstructed muscle volume (i.e., smaller muscles are more likely to be excluded).

Kappelman (1988) took the approach of grouping a suite of muscles together as a functional unit on the basis of their shared travel path around a joint. When estimating the moment arm of extensor muscles crossing the knee in bovids, for example, Kappelman (1988) considered all members of the Mm. quadriceps femoralis group collectively as having a shared moment arm, as they all converge on the

patellar tendon and pass over the surface of the patella at an equal distance from the joint center. A similar approach has also been taken when modelling the Mm. quadriceps femoralis group around the human knee (Herzog and Read, 1993). Likewise, when joint surfaces are modelled as cylinders in multibody dynamic packages, such as Gaitsym and OpenSim (http://opensim.stanford.edu/: Delp et al., 2007), the minimum value for the moment arms of all muscles passing around the joint will be constrained as the radius of the cylinder and hence will be equal (see Geometric Shapes, below). This incorporation of isolated muscles into functional groups is particularly important when musculoskeletal models are to be used as the basis for forward dynamic modelling of movement. In this scenario, the addition of each extra muscle increases the dimensionality of the optimal control search space and causes a huge increase in terms of the cost of the simulation (Sellers et al., 2013), and recent fossil gait simulation studies have therefore restricted themselves to modeling generic 'knee flexors' and 'hip extensors', for example (Sellers et al., 2009).

In extant taxa, however, the separate heads of a single muscle have occasionally been found to possess very different moment arms around the same joint (e.g., equine M. biceps femoris and M. gastrocnemius: Crook et al., 2010). Different subunits of a single muscle may therefore be recruited for a different function during activation (Ackland et al., 2008). The corollary of grouping muscles by function, therefore, is that it may be necessary to model a single muscle as two separate functional units, particularly when osteological evidence suggests the presence of two distinct heads. For example, Bates et al. (2012a) modeled two aspects of the M. iliofemoralis (cranial and caudal), corresponding to the M. iliotrochantericus caudalis and M. iliofemoralis externus, respectively, in extant birds. Even if both heads are

found to have similar moment arms, modelling them as separate muscle-tendon units allows for potential functional differentiation in future forward dynamic analyses.

Ultimately, the decision to group or to split muscles on the basis of function reflects a compromise between modelling the intricacy we know to characterize modern musculoskeletal systems, and the computing time and degree of uncertainty we must accept if we attempt to include such complexity into our models of extinct taxa.

Muscle Origins and Insertions—While some muscles are characterized by possessing discrete 'heads' as discussed above, others are large and fan-shaped with broad attachment sites lacking distinct segregations. Single lines of action spanning from origin to insertion cannot adequately describe the geometry of such muscles, and multiple lines of action with independent origins and insertions may need to be designated a priori (van der Helm and Veenbaas, 1991). Travel paths originating at opposing positional extremes within a given muscle are expected to pass across the joint at different locations, and therefore possess different values of muscle moment arm.

When subdividing fan-shaped muscles, the criteria for selecting the number and location of multiple lines of action are not always made clear, and may be related to position ('superficial' vs. 'deep'), perceived function, or selected in order to capture differing fiber directions within the muscle. The practice of partitioning muscles with large attachment sites is common in human biomechanical modelling (Delp et al., 1990; van der Helm and Veenbaas, 1991; Holzbaur et al., 2005; Chadwick et al., 2009; Arnold et al., 2010; Webb et al., 2012) and is increasingly applied to other extant taxa, particularly in MBDA of skull function (Wroe et al., 2007, 2013; Gröning et al., 2013; Watson et al., 2014). Modern studies benefit from

607 the incorporation of dissection data and MRI-based imaging of in-situ 3D muscle
608 geometry when subdividing muscles for this purpose. In contrast, the representation
609 of large muscles in paleontological models ranges from single lines of action (with the
610 origin located at the centroid of the attachment site: Ravosa, 1996), to separate bodies
611 representing the two extremes in attachment location (typically anterior-most vs.
612 posterior-most positions, or preacetabular vs. postacetabular: Hutchinson et al., 2005;
613 Bates et al., 2012a; Maidment et al., 2014a), to several lines of action (McHenry et al.,
614 2007; D'Anastasio et al., 2013; Gill et al., 2014).
615 To illustrate this point, we model the M. latissimus dorsi (LAT) of
616 *Stegosaurus*, a large fan-shaped dorsolateral muscle located posterior to the shoulder
617 joint that is responsible for humeral retraction (Meers, 2003; Dilkes et al., 2012). The
618 scapula is considered fixed relative to the trunk, and the shoulder is modelled as a
619 simple hinge joint permitting only flexion-extension. LAT is simplified into five lines
620 of action, originating from the neural spines and transverse processes of dorsal
621 vertebrae 3–7, travelling posterior to the shoulder joint and attaching at a common
622 insertion point on the posterior shaft of the humerus ventral to the head (Fig. 6).
623 Tendon length is, of course, another unknown parameter in model construction. If the
624 tendon of LAT was long, and the fibers of LAT merged onto the tendon prior to
625 passing around the shoulder joint, the LAT can be considered to have effectively a
626 single moment arm. However, assuming the tendon was short, LAT would have had
627 numerous lines of action around the joint, and therefore a range of moment arm
628 values. Travel paths were modified by via points located on the rib tubercula, lateral
629 margins of the dorsal ribs and the lateral surface of the scapula blade to prevent
630 intersection with the skeleton (see Muscle Paths, below).

631 Figure 6A (solid line) illustrates the variation in LAT moment arm with
632 humeral protraction-retraction. At maximum humeral protraction, LAT moment arm
633 values are low and decrease from the most posterior muscle line of action to the
634 anterior-most. At maximum humeral retraction, LAT moment arms are considerably
635 higher. As a percentage of LAT moment arm, divergence between anterior- and
636 posterior-most muscle lines of action is greatest at full humeral protraction, and at a
637 minimum at 40° retraction. Crucially however, the interpreted function of the muscle
638 remains consistent amongst these different lines of action. Whilst incorporating
639 multiple lines of action for a given muscle into a model will more adequately
640 represent the action of a muscle attaching over a large area of the bony surface (van
641 der Helm and Veenbaas, 1991), a single centroid-based muscle path appears sufficient
642 for describing the change in LAT moment arm with joint angle in this particular fossil
643 taxon. Comparisons of single muscle moment arms across taxa and between studies
644 therefore remain valid, but should be accompanied by a description of how the muscle
645 origin centroid was determined to improve the repeatability of the technique.
646 In many instances, muscle moment arm estimates may be more sensitive to
647 shifts in muscle insertion than origin. As in the case of the LAT (Fig. 6B–E), muscle
648 insertions are often closer to the joint center of interest than muscle origins. Shifting
649 the position of a muscle insertion by a given distance will therefore displace the
650 muscle line of action from the joint center further than an equal shift in the position of
651 muscle origin (O'Neill et al., 2013). In terms of myological reconstructions, the
652 insertion of the LAT on the posterior surface of the humerus has a particularly clear
653 osteological correlate in *Stegosaurus* (Maidment et al., 2015:fig. 67). Yet whilst the
654 LAT insertion on the latissimus tubercle is well constrained and small in size relative
655 to that of other pectoral muscles, the scar does extend up to 100 mm proximodistally.

In Figure 6D–E, the insertion of LAT has been shifted 50 mm to its proximal-most position on the humerus and Figure 6A (dashed line) illustrates the effect that this change has upon calculated moment arms. The impact of shifting LAT insertion site is negligible at full humeral protraction, and variation introduced through the positioning of muscle lines-of-action at the origin contributes more to variation in LAT moment arms. With increased humeral retraction, however, variability in moment arms due to insertion site position comes to dominate over variation due to muscle origin.

For the purpose of muscle moment arm estimation, this suggests that a shift towards concentrating on improving the identification of muscle insertion locations would be particularly beneficial (Hutchinson et al., 2014). Exceptions will exist, however, in which the joint center is located closer to muscle origin than insertion (as in the case of *Stegosaurus*, with the origins and insertions of the M. adductor group and M. iliotibialis muscles around the hip). This highlights the idiosyncratic nature of muscle modelling and emphasizes the need for a muscle-by-muscle approach to sensitivity analyses; the same parameters that might strongly affect the moment arm of one muscle may have little or no effect on neighboring muscles acting around the same joint.

Joint Definitions

Joint Centers—Given the geometric definition of a muscle moment arm as the perpendicular distance from joint center to the muscle-tendon unit line of action, it is crucial to accurately determine the position of the joint center when conducting moment arm analyses. Calculated moment arms have been found to vary considerably with estimated joint center in clinical human studies, and in some cases can result in a

shift in predicted function from flexion to extension (Herzog and Read, 1993). Delp and Maloney (1993) estimated that a 20 mm shift in the position of the human hip center may result in a change in percentage moment arms of between 0–38%, dependent upon the direction of shift and the axes about which the moment arms are measured.

Consequently, there is a considerable body of research on methods for accurately determining joint centers in modern taxa, which may be broadly subdivided into geometric and kinematic techniques. Kinematic joint centres are calculated on the basis of instantaneous helical axes, in which the motion of an object can be broken down into a rotation about and a translation along its rotational axis. Kinematic joint centers can be estimated in-vivo or in-vitro via the tracking of anatomical landmarks through the limb range-of-motion using motion capture (Sholukha et al., 2013) or biplanar fluoroscopy (Pillet et al., 2014).

Geometric joint centers are calculated on the basis of fitting simple geometric shapes to joint surfaces, derived from 3D coordinate measurement systems such as microscribes or computed tomographic (CT)/magnetic resonance imaging (MRI) data. Geometric joint centers are considered fixed throughout the range-of-motion, thus ignoring possible translation of one element relative to another (see Joint Type, below). In clinical human trials, joint centers calculated using kinematic and geometric techniques are in broad agreement (e.g., glenohumeral joint: Veeger, 2000; femoroacetabular joint: Klein Horsman et al., 2007; femorotibial joint: Eckhoff et al., 2003). As such, this technique can be considered applicable to disarticulated skeletons, including those of extinct taxa, for which kinematic data cannot be collected.

705 Within the paleontological literature, methodological descriptions of the
706 process of determining geometric joint centers range from detailed (Hutchinson et al.,
707 2005; Fujiwara and Hutchinson, 2012) to sparse (Sellers et al., 2013) or entirely
708 absent (Sellers et al., 2009; Maidment et al., 2014b). Typically, the femoroacetabular
709 joint is identified by fitting circles and spheres to the acetabulum and femoral head
710 respectively, and subsequently aligning their centroids (Hutchinson et al., 2005; Costa
711 et al., 2013). The center of the elbow has been similarly defined as the center of the
712 radial condyle and sigmoid notch on the humerus and radius/ulna respectively,
713 calculated through the process of geometric shape fitting (Fujiwara and Hutchinson,
714 2012). Likewise, the position of the knee joint centre has been estimated by fitting
715 circles to the medial and lateral condyles, and taking the midpoint of the axis joining
716 the centers of both circles (Hutchinson et al., 2005).
717 As discussed above, the loss of articular cartilage will undoubtedly affect the
718 position of the joint center calculated through the process of shape fitting. However,
719 given the lack of data on the thickness and distribution of cartilage in extant species, it
720 is difficult to account for in extinct taxa. Taphonomic distortion of the epiphyses may
721 also impact accurate identification of joint centers. Figure 7 demonstrates the process
722 of fitting circles to the medial and lateral femoral condyles of *Stegosaurus stenops*.
723 Figure 7A shows the considerable extent of taphonomic warping present in the distal
724 femoral condyles, in which the condylar long axes have been rotated away from the
725 anteroposterior axis of the femur mediolaterally. First, vertices were manually
726 selected in Meshlab along a line trending anteroposteriorly across the ventral surface
727 of both condyles (Fig. 7B), hence ignoring any taphonomic distortion. Selected
728 vertices were projected onto a sagittal plane cutting through the femur, and best-fit
729 circles were fitted to the coordinates (Fig. 7D–E.) using the ‘circle fit’ function from

730 MATLAB File Exchange (Bucher, 2004). The center of the knee joint was
731 subsequently calculated as the midpoint of the line connecting the centers of both
732 medial and lateral femoral circles. This process was repeated by selecting vertices
733 describing the main curvature of the condyles, thus taking the rotation of condylar
734 long axes into account (Fig. 7C), and fitting best-fit circles to the data (Fig. 7F–G).
735 When accounting for deformation, the condylar surfaces approximate a circle
736 more closely than when vertices are selected in a strict anteroposterior plane (Fig.
737 7D–E vs. Fig. 7F–G), the radii of the fitted circles increase considerably (medial
738 condyle radius increases 21%; lateral condyle radius increases 38%), and the
739 calculated position of the joint center shifts by 12.7 mm. The effect of this upon
740 calculated moment arms around the knee is discussed below. Given the sensitivity of
741 estimated joint centers to the manual selection of surface vertices, and to the presence
742 of taphonomic deformation, it is therefore essential that the process of calculating
743 joint centers be explicitly stated in the study methodology.
744 Furthermore, the *Stegosaurus* specimen presented here comprises a near-
745 complete skeleton, within which the extent of taphonomic deformation can be
746 accurately assessed and compared against other documented *Stegosaurus* individuals.
747 In contrast, when material is highly fragmentary or of uncertain taxonomic affinity,
748 the degree to which underlying morphology represents ‘normal’ or ‘taphonomic’
749 processes may be less clear. There is a well-established body of literature on the
750 technique of fossil ‘retrodeformation’ to account for taphonomic effects, and its
751 subsequent impact upon functional analyses. Thus far, these studies have generally
752 focused upon skull morphology, however (Lautenschlager et al., 2014; Cuff and
753 Rayfield, 2015; but see Motani, 1997). Future research should concentrate on the
754 postcranial skeleton, in particular the geometry of long bone epiphyses, to elucidate

the effects of fossilization and potential deformation upon interpreted skeletal function.

Joint Type—As outlined above, the geometric method of calculating joint center does not require kinematic data and is solely based upon the surface contours of the joint. This approach does, however, assume that the joint center remains fixed relative to the two bodies. Yet in reality, many joints are characterized by some degree of sliding (translation) in addition to pure rotation. Classically, movement in the knee joint has been found to comprise both rolling and sliding (Iwaki et al., 2002), with the condyles of the tibia sliding towards the extensor surface of the femur during knee flexion (Johnson et al., 2008). Translation at the knee joint has been incorporated into musculoskeletal models of modern humans (Steele et al., 2012) and chimpanzees (O'Neill et al., 2013) but has not, to the authors' knowledge, been investigated in fossil species.

Likewise, the glenohumeral joint of the shoulder is typically considered as a simplified ball-and-socket joint with minimal translation (Veeger and van der Helm, 2007). However, movement at the shoulder is a function of mobility at both the glenohumeral joint and the scapulothoracic gliding plane, and the medial border of the scapula remains in contact with, and translates/rotates relative to, the thoracic wall. The contribution of scapula motion to total arm elevation ('scapulohumeral rhythm') is relatively well known in modern humans (Inman et al., 1944; Bolsterlee et al., 2014), and a musculoskeletal model of the forelimb of Japanese macaques has incorporated scapula movement as a triaxial gimbal joint (Ogihara et al., 2009; although this model has thus far only been used in studies of bipedalism). However, this only provides a first approximation of the wide range of possible scapula motions, and again, we know of no paleontological musculoskeletal model in which

translation/rotation of the scapula is included. Similarly, biomechanical models of feeding in fossil taxa often assume a simplified hinge for the jaw joint (e.g., Bates and Falkingham, 2012; Wroe et al., 2013; Lautenschlager et al., 2015; but see Snively et al., 2015) despite some degree of translation and/or long-axis rotation being present in both mammal (Noble, 1973; Terhune et al., 2011) and reptile (Jones et al., 2012) jaws.

Currently kinematic data on joint translation in non-human species are extremely sparse and, as a result, any attempt to incorporate movement of the joint center into models of fossil species would be speculative. Furthermore, the importance of incorporating translation into joint mobility will vary across taxonomic groups (e.g., between mammals and archosaurs). In contrast, the calculation of a fixed center of rotation based solely on joint geometry is comparatively simple, repeatable and widely applicable across a broad range of paleontological specimens. Ultimately, the degree of complexity incorporated into fossil reconstructions should be a function of the question being considered. If the goal of a study is to generate the most 'accurate' model of a particular fossil joint, then an argument can be made for incorporating as much detail as possible on joint mechanics. If, however, the goal is to make broad comparisons of muscle function across a large sample of taxa, assuming a fixed joint center may be more feasible.

When ignoring the role of translation, musculoskeletal joints are typically modelled as fixed hinge joints with one degree of rotational freedom (as in the case of the elbow, knee, and jaw) or ball-and-socket joints with three degrees of rotational freedom (in the shoulder and hip). When assigning joint limits (i.e., the range of motion through which the limb may move), maximum and minimum joint angles are straightforward when assigned to hinge joints operating solely within one plane. In contrast, setting joint limits upon ball-and-socket joints can be considerably more

805 difficult. At the simplest level, Euler angles can be used to represent motion by three
806 rotations about three different axes. Independent limits can be specified on each Euler
807 angle, however the resulting range of motion has been shown to predict in-vivo
808 motion ranges poorly (Baerlocher and Boulic, 2001). Furthermore, Euler angles are
809 not particularly intuitive (two angles that appear intuitively close to each other may
810 not necessarily have similar Euler angles) and can be difficult to set at sensible values
811 (Sellers, 2014). For the purpose of calculating muscle moment arms in simple
812 anatomical planes, it may be more straightforward to define three orthogonal hinge
813 axes and restrict joint movement to one axis in turn, as opposed to defining true ball-
814 and-socket joints, and this also avoids the potential for gimbal lock.
815
816 **Muscle Paths**
817 At the simplest level, a muscle can be modelled as a straight line travelling
818 from origin to insertion (Fig. 1), and it is in this manner that early studies of muscle
819 moment arm (then more commonly referred to as 'lever arm') in fossils were
820 conducted (Miller, 1915; Fisher, 1945; Maynard Smith and Savage, 1956). An
821 advantage of this 'dry-bone' approach is that no assumptions regarding the travel path
822 of the muscle are required, and calculations are based solely upon muscle scarring and
823 estimated joint centers. Furthermore, the data collection process involves
824 straightforward measurements of bone geometry and sample sizes can therefore be
825 large. Recently, a study used a similar idealized origin-insertion model to calculate
826 muscle moment arms around the elbow in a large dataset (n = 318) of extant and
827 extinct tetrapods (Fujiwara and Hutchinson, 2012). Similar sample sizes are currently
828 unachievable when calculating moment arms on the basis of articulated 3D digital
829 models.

However, many studies seek to quantify changes in muscle moment arms with joint angle, and must therefore accommodate complex muscle geometries and muscle paths that shift as the limb moves through its range of motion. In the case of a 3D reconstruction of *Homo neanderthalensis* hamstring muscle paths were modelled as straight lines and did not intersect with the skeleton throughout the range of knee flexion angles considered (Chapman et al., 2010). In most instances, however, the path from origin to insertion is not linear (Gröning et al., 2013). Muscles must therefore be wrapped around objects, or constrained to travel through predetermined points, in order to prevent intersection with the skeleton or unrealistic 'bow-stringing' away from the bone surface (Murray, 1995). This is referred to as the 'centroid approach' (Garner and Pandy, 2000) in which a muscle path is represented as a curving line connecting cross-sectional centroids along the muscle's length.

Figure 8A illustrates the problem of muscle paths intersecting with the skeleton. The M. iliotibialis 1 (ILT1) was reconstructed as travelling in a straight line from its origin on the dorsal ilium to its insertion on the cnemial crest on the tibia. With knee flexion, ILT1 implausibly intersects the skeleton and migrates caudally to the joint centre of rotation, shifting the interpreted muscle function from knee extensor to knee flexor. This highlights the utility of multibody dynamic software packages with graphical user interfaces (GUIs) that allow the user to visualize the model and resulting simulations. It is crucial that the user manually inspects the travel path of each muscle as the limb is moved through its full range of motion in order to detect any potential issues with muscle wrapping or joint impingements. A concern when running numerical musculoskeletal simulations without accompanying visualizations is the ease with which models can be created, and properties assigned, that would otherwise immediately appear unfeasible if the data were viewed as an

855 articulated skeleton. The process of visually inspecting muscle paths is time
856 consuming, but essential in order to achieve meaningful values for estimated moment
857 arms. In addition, when musculoskeletal models are to be used for MBDA, muscle
858 wrapping has been found to have a notable effect on force generation and the
859 inclusion of complex wrapping (as opposed to straight line origin-insertion) can bring
860 force estimates closer in line with in-vivo measured values (Gröning et al., 2013).
861 The specific options available for modifying the path of a muscle vary
862 between software packages (e.g., Gaitsym vs. OpenSim; see later discussion).
863 Regardless, a compromise will always exist between anatomical accuracy and muscle
864 paths that can be achieved feasibly within the constraints of the modeling software.
865 Two broad categories for describing changes in muscle path have been used: via
866 points and geometric shapes.
867 **Via Points**—Via points constrain the muscle to pass frictionlessly through a
868 specific point in space as defined by Cartesian coordinates, acting as retinacula (Delp
869 et al., 1990). By assigning several via points, complicated muscle paths can
870 effectively be divided into a series of straight-line segments. Figure 8B–C illustrates
871 the path of the M. ischiotrochantericus (ISTR) from its origin on the medial surface of
872 the ischium to its insertion on the proximolateral femur. In this instance, three via
873 points (one on the posterodorsal margin of the ischium and two on the lateral margin
874 of the femur) were necessary to prevent the ISTR from intersecting the skeleton
875 throughout the limb's full range of motion.
876 Via points are problematic for a number of reasons, however. By constraining
877 the muscle to pass through a given xyz location, the muscle is prevented from sliding
878 across the bony surface. Furthermore, the moment arm of a muscle around a given
879 joint will be entirely determined by the location of via points fixed immediately to

880 either side of that joint. In other words, when via points are used to subdivide a
881 complicated muscle path into a series of straight line segments, the calculated moment
882 arm is that of the segment running across the joint in question, as opposed to a
883 reconstructed muscle running the entire anatomical distance from origin to insertion.
884 Osteological evidence of muscle scarring at origin and insertion sites may not,
885 therefore, contribute directly to the calculated moment arms. Instead, the positioning
886 of via points (which are byproducts of the modeling approach) can heavily influence
887 estimated moment arms.
888 When defining via points, it is necessary to specify the body segment to which
889 they will remain fixed during limb movement. In some instances, when a via point
890 replicates the behavior of a retinaculum located on the bony surface, for example, the
891 appropriate body segment is clear. In other scenarios, via points may be a fixed point
892 in space, some distance from the skeleton (Bates et al., 2012a:fig. 2G around the knee
893 joint of *Lesothosaurus diagnosticus*; Maidment et al., 2014a:fig. 2A–H around the
894 knee joint of several ornithischian dinosaurs). In the aforementioned studies, only
895 muscle moment arms around the hip are calculated. Figure 9 illustrates the behavior
896 of IFB when via points are employed in a similar manner to modify the muscle path
897 around the knee during knee flexion.
898 Two IFB muscles are included here, both originating and inserting at the same
899 location as described in Figure 9, and both passing through the same via point located
900 posterior to the knee joint center. The two IFB models differ in the body segment to
901 which the via point is fixed; one remaining fixed relative to the femur (IFB_f), and the
902 other fixed to the tibia (IFB_t). With knee flexion, the paths of IFB_f and IFB_t diverge
903 (Fig. 9). When remaining fixed relative to the femur during joint rotation, the IFB_f

904 impinges on the posterior surface of the tibia, whilst the IFB_t via point remains
905 stationary relative to the tibia and intersects the posterior surface of the femur.
906 The knee is a fairly straightforward case in which a clear biomechanical
907 argument could be made for the femur being the most appropriate body segment upon
908 which to attach the IFB via point, due to the likely location of the knee joint center
909 within the distal femoral condyles. In other cases, however, such as the neck, spine,
910 and ribcage, the decision as to which rigid body segment to kinematically link the via
911 point can be more ambiguous. Additionally, Sellers (2014) raises concerns regarding
912 the unrealistic behavior of via points at extreme values of joint rotation (as in Fig. 9),
913 and Garner and Pandy (2000) highlight the potential for discontinuities in moment
914 arms to occur when calculated across joints with more than one degree of freedom.
915 **Geometric Shapes**—As an alternative to via points, 'obstacle set' wrapping
916 (Garner and Pandy, 2000) seeks to represent anatomical features (such as bony
917 surfaces and underlying soft tissues) as simple geometric shapes including spheres,
918 cylinders, and toroids. Coordinates describing the surface contours of a joint may be
919 collected from CT/MRI, or via the use of a digitizing probe or microscribe on
920 cadaveric or dry skeletal material. Shapes may then be fitted to the bony landmarks
921 using an optimization process (Van der Helm et al., 1992) or via simple best-fitting of
922 circles as illustrated in Figure 7.
923 In contrast to via points, geometric shapes do not constrain a muscle to pass
924 through a specific xyz position in space, and instead allow the muscle to slide across
925 the surface of the object. Within the paleontological literature, cylinders are most
926 often deployed at the epiphyses of long bones to replicate the wrapping path of
927 muscles around the condyles (Hutchinson et al., 2005; Sellers et al., 2013). Typically,
928 the axis of a cylinder is constrained to pass through the joint center, with the long axis

929 of the cylinder aligned mediolaterally. The radius of the object can then be set to
930 approximate the contours of the joint surface. Alternatively, geometric shapes can be
931 used to wrap around other bony features distant from the joint surface. For example,
932 Klein Horsman et al. (2007) used cylinders to replicate the wrapping of the M.
933 iliopsoas around the pubic bone in a musculoskeletal model of the human lower
934 extremity. Figure 10 illustrates the use of cylinders to wrap the M.
935 puboischiofemoralis internus (anterior and posterior) around the prepubis of
936 *Stegosaurus,* without which the muscles intersect with the skeleton implausibly. In
937 this instance, the cylinder is not constrained to an anatomical axis and is instead
938 aligned to a particular bony feature.
939 When using cylinders to approximate joint contours, the appropriate joint
940 center and cylinder radius may be calculated via the process of circle fitting to the
941 condylar surface (as outlined above). If taphonomic damage has occurred simple
942 geometric shapes may be used to reconstruct the former extent of underlying bony or
943 soft tissues. The impact that such retrodeformation may have upon estimated moment
944 arms will vary on a muscle-by-muscle basis. In Figure 11 we reconstruct the path of
945 the M. flexor tibialis externus (FTE) in *Stegosaurus*. Figure 11B illustrates the
946 original model, in which no attempt has been made to correct for the occurrence of
947 taphonomic deformation. Medial and lateral condyle cylinder radii and joint center
948 were calculated as outlined in Figure 7B, D–E. Alternatively, Figure 11C illustrates
949 the path of FTE when wrapped around a modified joint center with cylinders
950 accounting for the effect of deformation, as detailed in Figure 7C, F–G. As seen in
951 Figure 11A, calculated moment arms for FTE are relatively insensitive to the presence
952 of taphonomic damage at the condyles. Beyond 5° of knee flexion, the path of FTE no

953 longer wraps around the knee joint cylinder, and any discrepancy between models is
954 entirely due to a small shift in the joint center of rotation.
955 By contrast, when both muscle origin and insertion are located close to the
956 joint of interest, the muscle path may wrap around the fitted joint cylinder throughout
957 most of the joint's range of motion. In *Stegosaurus,* the M. femorotibialis lateralis
958 (FMTL) originates on the lateral femoral shaft and attaches to the cnemial crest of the
959 tibia (Fig. 12B). As illustrated in Figure 12A, the moment arm of FMTL remains
960 constant through the entire range of motion of the knee as the path of the muscle
961 remains tightly wrapped around the knee joint cylinder. Furthermore, the value of the
962 moment arm is exactly equal to the radius of the object around which it is wrapped.
963 The phenomenon of constant muscle moment has been noted previously (Hutchinson
964 et al., 2005), highlighting the sensitivity of calculated moment arms to the estimated
965 size of the joint cylinders. In the case of the FMTL, accounting for deformation of the
966 femoral condyles results in a 28% increase in calculated moment arm throughout the
967 full range of motion at the knee.
968 Muscles modeled as wrapping around cylinders do appear to behave better (in
969 terms of avoiding skeletal impingement or unrealistic travel paths) than those
970 modeled with via points, particularly at extreme joint angles. A recent
971 musculoskeletal model of an extinct sauropod (Sellers et al., 2013) avoided the use of
972 via points altogether, opting instead for simplified geometric wrapping surfaces at the
973 joints. Regardless of the particular path modifier chosen, muscle function is often
974 assumed a priori when determining the path of a muscle. For example, when
975 wrapping a muscle around a cylinder, the direction of wrapping must be manually
976 assigned. In Figure 11B, the FTE has been explicitly modeled as travelling posterior
977 to the joint center and the associated wrapping cylinder, and its function has therefore

been constrained as a knee flexor. Therefore, whilst the general aim of many fossil moment arm studies is to investigate muscle 'function', it must be recognized that the broad function of many muscles (i.e., flexor vs. extensor) has already been predetermined by virtue of the wrapping parameters chosen, and the EPB-based myology upon which the model is based.

Finally, the layering of neighboring soft tissues such as muscle and tendon may also be taken into consideration when defining individual muscle paths and wrapping. Several studies calculating muscle moment arms have attempted to account for this effect, with inferior muscles wrapping closer to joint surfaces than those lying superior (Hutchinson et al., 2005). However, estimates of the likely thickness of underlying muscle and tendon in fossils should be based on modern dissection data, of which little has been published outside the clinical literature. Additionally, our current models cannot account for shortening and thickening during contraction in surrounding soft tissues and any potential effect that this may have upon calculated moment arms. As such, it would be prudent to restrict modeling to individual muscle-tendon units in isolation from other neighboring soft tissues, in order to minimize subjectivity and improve repeatability in model creation.

Biarticular Muscles—Several of the muscles included in the present model are biarticular (i.e., span more than one joint). In common with most modern cadaveric analyses of muscle moment arms (e.g., Channon et al., 2010), here we fix the additional joint whilst manipulating the joint of interest through its range of motion. Elsewhere, calculated muscle moment arms around the ankle have been shown to be relatively insensitive to knee flexion (Holokwa and O'Neill, 2013). This suggests that the simplification of fixing additional joints may not unduly affect

1002 calculated moment arms around joints of interest, although further data from living
1003 taxa are required to confirm this.
1004 It must also be recognised that a biarticular muscle moment arm around one
1005 joint will be sensitive to the wrapping parameters of a neighbouring joint. Moment
1006 arms calculated around the knee, for example, are determined in part by the position
1007 of the hip wrapping surface, which is itself a function of the hip joint center location
1008 and wrapping geometry. Uncertainty in one joint can therefore permeate calculations
1009 of moment arms around neighbouring joints. In the case of biarticular muscles,
1010 sensitivity analyses may therefore benefit from incorporating uncertainty in both
1011 joints.
1012
1013 INTER- AND INTRASPECIFIC VARIATION IN MUSCLE MOMENT ARMS
1014
1015 **Making Interspecific Comparisons between Fossil Taxa**
1016 The foregoing discussion considers how the muscle moment arms of a single
1017 fossil individual may be calculated. Yet absolute values for the moment arms of a
1018 single individual are rarely of interest. Rather, comparative studies of numerous fossil
1019 species may be undertaken in order to quantify changes in muscle function within or
1020 between lineages, or higher order biomechanical variables assessed via forward
1021 dynamics approaches. When comparing a linear metric such as muscle moment arm
1022 between species, geometric similarity would predict absolutely larger animals to
1023 possess larger moment arm values. Therefore, in order to tease functional signals and
1024 overall body size signals apart, it is necessary to normalize muscle moment arm
1025 values.

1026 Osteometric scaling is a well-established practice in the human clinical
1027 literature (Sommer et al., 1982; Duda et al., 1996), and facilitates inter-specimen
1028 comparisons of muscle attachment sites. In comparative studies across modern taxa,
1029 limb muscle moment arms have been scaled by segment length (that is, moment arms
1030 calculated around the hip and knee are normalized to femur length, whilst those
1031 around the ankle are normalized to tibia length) (Payne et al., 2006; Crook et al.,
1032 2010). This methodology has been applied to hind limb muscle moment arms
1033 calculated for comparative samples of dinosaur taxa (Bates et al., 2012b; Maidment et
1034 al., 2014a). Likewise the moment arms of jaw muscles acting around the
1035 temporomandibular joint have been normalized to mandible length in extant (Smith
1036 and Redford, 1990) and extinct (Vizcaíno and Iuliis, 2003) species.
1037 The motivation behind normalizing muscle moment arms by segment length is
1038 often to control for 'body size'. By removing size-related signals from moment arm
1039 data, any functional signals of interest will become more apparent. When dividing
1040 muscle moment arms calculated around the hip by femoral length, for example, there
1041 is an assumption that femoral length is strongly correlated to overall 'body size' and
1042 does not itself contain a functional signal. Yet this is not the case. Several independent
1043 studies have found long bone length is often a less accurate predictor of body mass in
1044 modern vertebrates relative to cross-sectional properties (Damuth and MacFadden,
1045 1990; Campione and Evans, 2012), and segment length may contain a strong
1046 functional signal (Brassey et al., 2013). The elongated zeugopodium of modern
1047 wading birds is an extreme example.
1048 When attempting to remove 'body size' from an analysis of moment arms, a
1049 metric known to be highly correlated with body mass in modern species (such as
1050 stylopodial circumference or diameter: Campione and Evans, 2012; Brassey et al.,

1051 2013) could be applied to normalize the data. Figure 13 illustrates the effect of
1052 normalizing moment arm values calculated for the M. caudofemoralis longus (CFL)
1053 around the hip in *Stegosaurus* and *Kentrosaurus aethiopicus* (see Maidment et al.,
1054 2014a for model details), a smaller Late Jurassic stegosaurian. By normalizing CFL
1055 moment arms by linear dimensions of the femur, values for the two species are
1056 brought into closer agreement. Whilst the rank order of the two species does not
1057 change (*Stegosaurus* consistently has larger values for CFL moment arm than
1058 *Kentrosaurus*), the extent of the divergence between the two species does differ
1059 depending upon the normalizing metric applied. Peak CFL moment arms in
1060 *Stegosaurus* are 19% greater than those of *Kentrosaurus* when normalizing to femur
1061 length, compared to 38% when normalizing to anteroposterior diameter (Fig. 13B vs.
1062 Fig. 13D).

1063 However, this approach still requires a judgment to be made regarding which
1064 skeletal metric should be preferred. Alternatively, an osteometric scaling approach
1065 based on procrustes superimposition of skeletal elements could be applied to remove
1066 the effects of translation, rotation, and scaling, and quantify the impact of changes in
1067 bone geometry and attachment sites on muscle moment arms. A geometric mean of
1068 several skeletal variables could also be used. In reality, however, the occurrence of
1069 taphonomic damage and weathering may preclude the application of a particular
1070 metric to a given group of fossils, and normalization of a dataset should be considered
1071 on a case-by-case basis. To facilitate future comparisons, the process of moment arm
1072 normalization should be explicitly described in the methodology. In addition, the
1073 potential for the normalization process to change the rank order of calculated moment
1074 arms within the sample should be recognized.
1075

Intraspecific Variation in Moment Arms

In addition to interspecific differences, evidence from the clinical literature suggests that within-species variation in muscle moment arms can also be considerable. In human adults, the relationship between moment arm and joint angle typically describes an overall similar curve between individuals, whilst possessing different absolute values (in the knee: Herzog and Read, 1993; and elbow: Murray et al., 2002). Much of the difference in absolute values is attributed to intraspecific variation in total body size. Yet, despite performing osteometric scaling on the basis of markers and reference points, Duda et al. (1996) still found considerable differences in the position of femoral muscle attachment centroids across a sample of humans, resulting in moment arm standard deviations of up to 65% of the mean in some muscles. Therefore, even when accounting for changes in overall body size, intraspecific variation in muscle attachment sites is likely to be present in calculated muscle moment arms.

Outside of humans, few data exist for extant taxa regarding within-species variation in attachment sites and muscle moment arms (but see Smith et al., 2007). Within the body of available data, confounding epigenetic factors confuse matters further, including adaptations in response to exercise regimes in captive zoo animals and domesticated species. Ontogeny also has an impact on moment arms, with muscles shifting their location relative to one another, and to the joint they act around, with age (Carrier, 1983; Young, 2005; Singleton, 2015). The moment arms calculated herein for a subadult *Stegosaurus* specimen, for example, may not be directly comparable to those of a mature individual of the same species, or to adult specimens of closely related taxa.

Intraspecific variation is rarely considered in paleontological musculoskeletal reconstructions, however, due either to lack of specimens or constraints associated with the time-consuming process of model creation. Yet given the substantial inconsistency in muscle attachment positions (and hence moment arms) in modern humans, further research into the relative magnitudes of inter- and intraspecific variability in moment arms across modern comparative samples may be necessary. If between-species variation in moment arms is found to dwarf that within-species, then we may have more confidence in attributing patterns in calculated moment arms of fossil species to functional shifts within lineages.

VERIFICATION AND VALIDATION OF MUSCLE MOMENT ARM MODELS

The discussion provided above outlines the process of generating musculoskeletal models for fossil taxa from which muscle moment arms may then be calculated. Yet, in addition to creating an accurate 3D representation of a fossil skeleton and associated musculature, it is important to verify and validate model results. In their review of computational modeling of the neuromusculoskeletal system, Hicks et al. (2014) considered the best practices for verifying and validating biomechanical models of muscles and movement. These authors emphasized the difference between verifying MDBA software ('are we solving the equations correctly?') and validating model results ('are we solving the correct equations?').

Verification

For users, the process of verifying whether or not MBDA software is implementing algorithms correctly has been mostly completed. When employing

well-established software modules (either commercial or open source), most source code has been independently verified by an extensive user community. Commercial packages such as SIMM (Delp et al., 1990), Adams (MSC Software Corp.), and AnyBody (AnyBody Technology) have already been successfully applied to a wide spectrum of biomechanical problems, including non-human extant taxa (frog: Kargo and Rome, 2002; horse,:Brown et al., 2003; tuatara: Curtis et al., 2010; rat: Wehner et al., 2010; rabbit: Watson et al., 2014; pigs: Basafa et al., 2014) and occasionally fossils (Hutchinson et al., 2005; Snively et al., 2013).

The above-mentioned software packages do not, however, provide full access to the source code. OpenSim (Delp et al., 2007) and GaitSym (Sellers, 2014) are open-source alternatives. OpenSim uses SimBody as its physics engine, and has been applied in numerous non-human studies, including the macaque forelimb (Schaffelhofer et al., 2015), and chimpanzee (O'Neill et al., 2013), sheep (Lerner et al., 2015), and rat (Johnson, 2009) hind limbs. Likewise, Gaitsym is open-source and uses the Open Dynamics Engine (ODE) physics library to perform most rigid body dynamics calculations. Gaitsym (and its precursors) have been applied to MBDA of both extant (human: Sellers et al., 2010; chimpanzee: Sellers et al., 2013) and extinct (hominoid: Nagano et al., 2005; Sellers et al., 2005; dinosaur: Sellers and Manning, 2007; Bates et al., 2012a, b; Maidment et al., 2014a) taxa.

A recent study comparing the results of MDBA run using various physics engines (including ODE, Bullet, and Simbody) reassuringly found only minor differences in performance when applied to a simple walking task (Peters and Hsu, 2014). However, as far as we are aware, a straightforward comparison of moment arm values calculated for equivalent musculoskeletal models across different MBDA software packages has yet to be attempted. Such a comparison could potentially prove

interesting, as current MBDA packages differ considerably in the muscle wrapping parameters available to users. For example, while muscles may be modelled as wrapping around toroids in OpenSim, GaitSym only allows muscle wrapping around cylinders. Models created in one package may not, therefore, be directly imported and verified in another. Finally, 3D moment arm calculations are essentially simple trigonometry problems, and may be verified using back-of-the-envelope calculations. Moment arm values calculated from detailed 3D musculoskeletal models employing complex muscle-wrapping should therefore be verified using this simplified approach to ensure that both techniques converge on similar results.

Validation

Validating the outputs of musculoskeletal models for extinct species is obviously impossible. Therefore, for a biomechanical reconstruction technique to be considered reliable when employed in paleontology, its validity can only be approximated by applying it to relevant extant taxa (Hutchinson, 2011). When attempting to validate techniques for calculating muscle moment arms and inferring muscle function, we can ask the following questions related to modern taxa: 1) do muscle moment arms calculated using musculoskeletal models agree with experimental values?; and 2) do calculated muscle moment arms contain an obvious functional signal?

How do Muscle Moment Arms Calculated using Musculoskeletal Models Compare with those Measured Experimentally?—Within clinical biomechanics, there exists a substantial body of research comparing moment arm estimates derived from mathematical models to those estimated experimentally, due to the considerable advantages associated with avoiding invasive procedures or dissections. Numerous

1175 studies have found human moment arm estimates calculated from 3D computer
1176 models to fall consistently within the range of empirical data, for both ‘simple’ hinge
1177 joints such as the elbow (Murray et al., 1998) and more 'complex' joints including the
1178 knee (Arnold et al., 2000; Gatti et al., 2007). In non-human studies, a similar pattern
1179 is present in the hip and knee joints of frogs (Kargo and Rome, 2002) and
1180 chimpanzees (O’Neill et al., 2013), and the distal forelimb of horses (Brown et al.,
1181 2003), in which moment arms estimated from 3D musculoskeletal models have been
1182 found to be well-matched to those calculated experimentally, typically via the tendon-
1183 travel method. In some situations, it has been suggested that 3D modeling may be
1184 preferable to the tendon-travel method, due to the potential for muscle lines-of-action
1185 to be altered through the process of excising surrounding soft tissues during dissection
1186 (Hutchinson et al., 2015). Thus, the broad agreement between experimental and
1187 model results in extant taxa supports musculoskeletal modeling as a valid approach to
1188 calculating muscle moment arms in extinct taxa assuming a reliable myological
1189 reconstruction is available. The modern studies cited above rely upon detailed
1190 dissection data to inform the model-making process, something that is obviously
1191 unobtainable for fossil taxa. Whilst the agreement between techniques gives us
1192 confidence in 3D models as a means of calculating moment arms, musculoskeletal
1193 modeling is still subject to the phenomenon of ‘Garbage In, Garbage Out’ (GIGO),
1194 and the value of the moment arms output is directly a function of the quality of the
1195 myology upon which the model is based.

1196 **Functional Signals in the Muscle Moment Arms of Extant Species**—For a
1197 given property to be informative when applied to the fossil record, it must be first
1198 understood in extant taxa. In the case of muscle moment arms, values derived from
1199 fossil species are rarely of interest in and of themselves, but are instead used as a

1200 proxy for musculoskeletal function. Yet, as highlighted by Gans and De Vree
1201 (1987:76): “It remains necessary to check whether sites at which muscles are placed
1202 differ interspecifically and whether the functional […] implications of these
1203 differences match possible differences in role. If they do not, it is likely that the
1204 character state reflects phylogeny more than function”. Whilst dissection-based
1205 myological descriptions have a rich history in the field of modern comparative
1206 anatomy, and muscle moment arms are increasingly reported, the relationship
1207 between gross muscle architecture and muscle function across broad comparative
1208 datasets remains less than clear.

1209 In some instances, the calculated muscle moment arms of extant taxa may
1210 contain a functional signal. Rat hind limb muscle moment arms have been found to
1211 vary considerably throughout the physiological limb range of motion, yet peak and
1212 remain relatively constant within the range of motion domain occupied during
1213 locomotion (Johnson et al., 2008), implying moment arms may be indicative of
1214 dynamic limb posture. A caveat is that most rodent locomotion studies, such as
1215 Johnson et al. (2008), rely upon skin markers for their kinematics, which may poorly
1216 reflect the behavior of the underlying joints (Bauman and Chang, 2010). Likewise, the
1217 hardness of food items has been shown to influence mandible shape, and hence the
1218 mechanical advantage (ratio of the inlever and outlever) of several masticatory
1219 muscles in laboratory mice (Anderson et al., 2014), implying jaw muscle moment
1220 arms may correlate to dietary preference. Yet elsewhere, the moment arms of ostrich
1221 hind limb antigravity muscles calculated via 3D modeling were not found to peak at
1222 angles corresponding to mid-stance of walking and running during gait trials
1223 (Hutchinson et al., 2015), suggesting that there may not be a straightforward
1224 relationship between limb posture during stance phase and moment arms.

Additionally, the functional characteristics of muscle architecture can be studied on three levels (Gans and De Vree, 1987): 1) muscles within the organism; 2) fibers within the muscle; and 3) sarcomeres within the fibers. While paleontologists are restricted to the reconstruction of gross myology, there is mounting evidence that organisms primarily adapt their musculature to prevailing biomechanical conditions by changing intrinsic muscle properties. An increase in muscle moments within the limbs of sprinting racehorses relative to endurance horses has been attributed to increased muscle volume and physiological cross-sectional area rather than moment arm, for example (Crook et al., 2010). Similarly, modern gibbons have been found to employ a variety of compromises between fiber length and moment arm in order to achieve diverse biomechanical objectives (torque vs. control) within the hind limb (Channon et al., 2010), and adaptation to different feeding strategies in feline jaw muscles has been identified primarily in muscle fiber length (Hartstone-Rose et al., 2012).

In reality, the potential for a muscle to produce a moment is a function of both its moment arm and its ability to generate force, which is itself influenced by muscle size and internal organization. It may, therefore, be the 'totality' of the muscle architecture that is under the influence of selection (Gans and De Vree, 1987), without a well-defined relationship between one particular variable (such as moment arm) and a given function. Until a correlation between moment arm and function can be broadly identified across a range of modern taxa, the interpretation of moment arms calculated for extinct taxa should be approached with caution (Maidment et al., 2014a).

SUMMARY

In the preceding discussion, we outline the process of generating a musculoskeletal model for the purpose of muscle moment arm calculations in fossil specimens. In doing so, we highlight the model parameters to which calculated moment arms are particularly sensitive or robust. As a field, paleontology is increasingly engaging with methods of specimen digitization and musculoskeletal simulation and it is tempting to create ever more detailed and sophisticated models of extinct species. It is crucial, however, that our desire to generate 'realistic' models of fossil taxa does not outstrip the extent to which we may make reasonable inferences regarding the individual, and that we avoid becoming so 'seduced' by a technique that we might end up with models we no longer understand (Anderson et al., 2011).

It is beneficial, therefore, to refer back to the hierarchy of biomechanical questions outlined in the Introduction, to which muscle moment arm analyses are frequently applied. When utilizing musculoskeletal models to predict the role of an individual muscle around a joint (e.g., flexor vs. extensor), we might reasonably have confidence in the interpretation of muscle moment arms, as uncertainty in factors such as wrapping cylinder radii or joint center location are unlikely to change the fundamental action of a muscle. Variation in such parameters will impact upon moment arm magnitudes, however, and thus may change the rank order of individuals within a broad interspecific sample and fundamentally affect the interpretation of a dataset. Consequently, it is currently unclear whether moment arm analyses may be appropriately applied to test broader evolutionary hypotheses regarding changes in biomechanical function between lineages. Furthermore, the functional signal contained within the moment arms of extant species can often be contradictory. Until the methodology outlined above for the calculation of muscle moment arms can be

shown to reliably illuminate aspects of biomechanical function in extant taxa, paleontological studies of moment arms are being held at an “impasse” (Hutchinson et al., 2015:1).

Looking to the future, it is worth considering how we wish to use muscle moment arm data when applied to the fossil record. Is it important to understand the mechanical signal contained within muscle moment arm data? Or can muscle moment arms be used in a purely statistical sense, as a correlate for another parameter of interest? And, if the latter is the case, are complex models and simulations required to capture this data? 3D musculoskeletal models are still labor intensive, and their usage necessarily restricts sample sizes. If the aim of analysis is simply to ‘bin’ extinct species into disparate categories, such as ‘cursorial vs. digging’, or ‘upright vs. sprawling’, discriminant analyses on modern datasets of 2D moment arms may be more appropriate. Such analyses may be based on straightforward linear osteological measurements (Fujiwara and Hutchinson, 2012), facilitating the collection of large modern datasets without the need for extensive dissections or complex 3D muscle wrapping paths in our models. Statistical analyses such as these would also allow confidence limits to be ascribed to any predictions of potential function.

Alternatively, if 3D musculoskeletal models are favored, muscle moment arms may simply be a ‘means to an end’ for calculating other meaningful biomechanical parameters using powerful tools such as FEA, inverse- or forward MBDA. In this instance, muscle moment arms do still function as statistical correlates for the maximum moment-generating capacity of muscles. Such analyses can provide important insights into the functioning of muscle groups during locomotion, and may even generate gaits de novo. These studies do, however, require additional assumptions regarding the physiological cross-sectional area of muscles, fiber and

tendon lengths, and muscle activation patterns. Fundamentally, the quality of the fossil and the existence of modern analogues with associated anatomical data should dictate the complexity of the question being addressed, and by virtue the detail required within the model.

Moving forward, it is also essential that moment arm analyses pass the fundamental test of reproducibility. Previous paleontological studies have claimed that comparisons between musculoskeletal models may be easily made, as the 3D moment arm technique is quantifiable and repeatable (Maidment et al., 2014a). However, the extent to which moment arm calculations are reproducible has rarely been confirmed (although see Bates et al., 2012a). In addition to inter-observer variation in the interpretation and implementation of a given myology, variation in wrapping parameters between MBDA software packages makes repetition of results across studies challenging. Future studies should seek to standardize the reporting of musculoskeletal model parameters, in order to facilitate data sharing and model reproducibility.

ACKNOWLEDGMENTS

We are grateful for the insightful comments of Matthew Bonnan, John Whitlock, and one anonymous reviewer. The authors would also like to thank Bill Sellers for useful discussions and for his efforts in creating and maintaining GaitSym. We also express our sincere thanks to Jeremy Herrmann and the 69 other donors who made acquisition of the *Stegosaurus* specimen possible.

LITERATURE CITED

Ackland, D. C., D. Pak, M. Richardson, and M. G. Pandy. 2008. Moment arms of the muscles crossing the anatomical shoulder. Journal of Anatomy 213:383–390.

Alexander, R. M. N. 1989. Dynamics of dinosaurs and other extinct giants. Cambridge University Press, Cambridge, 167pp.

Alexander, R. M. N. 2003. Principles of Animal Locomotion. Princeton University Press, New Jersey, 384 pp.

An, K. N., K. Takahashi, T. P. Harrigan, and E. Y. Chao. 1984. Determination of muscle orientations and moment arms. Journal of Biomechanical Engineering 106:280–282.

Anderson, P. S. L., and M. W. Westneat. 2009. A biomechanical model of feeding kinematics for *Dunkleosteus terrelli* (Arthrodira, Placodermi). Journal of Paleontology 35:251–269.

Anderson, P. S. L., S. Renaud, and E. J. Rayfield. 2014. Adaptive plasticity in the mouse mandible. BMC Evolutionary Biology 14:85. DOI: 10.1186/1471-2148-14-85.

Anderson, P. S. L., J. A. Bright, P. G. Gill, C. Palmer, and E. J. Rayfield. 2011. Models in palaeontological functional analysis. Biology Letters 23:119–122.

Arnold, A. S., S. Salinas, D. J. Asakawa, and S. L. Delp. 2000. Accuracy of muscle moment arms estimated from MRI-based musculoskeletal models of the lower extremity. Computed Aided Surgery 119:108–119.

Arnold, E. M., S. R. Ward, R. L. Lieber, and S. L. Delp. 2010. A model of the lower limb for analysis of human movement. Annals of Biomedical Engineering 38:269–279.

1349 Astley, H. C., and T. J. Roberts. 2012. Evidence for a vertebrate catapult: elastic
1350 energy storage in the plantaris tendon during frog jumping. Biology Letters
1351 8:386–389.
1352 Baerlocher, P., and R. Boulic. 2001. Parametrization and range of motion of the ball-
1353 and-socket joint. IFIP Advances in Information and Communication
1354 Technology 68:180–190.
1355 Bargo, M. S. 2001. The ground sloth *Megatherium americanum*: Skull shape, bite
1356 forces, and diet. Acta Palaeontologica Polonica 46:173–192.
1357 Basafa, E., R. J. Murphy, C. R. Gordon, and M. Armand. 2014. Modeling the
1358 biomechanics of swine mastication - An inverse dynamics approach. Journal of
1359 Biomechanics 47:2626–2632.
1360 Bates, K. T., and E. R. Schachner. 2011. Disparity and convergence in bipedal
1361 archosaur locomotion. Journal of The Royal Society Interface 9:1339–1353.
1362 Bates, K. T., and P. L. Falkingham. 2012. Estimating maximum bite performance in
1363 *Tyrannosaurus rex* using multi-body dynamics. Biology Letters 8:660–664.
1364 Bates, K. T., R. B. J. Benson, and P. L. Falkingham. 2012b. A computational analysis
1365 of locomotor anatomy and body mass evolution in Allosauroidea (Dinosauria:
1366 Theropoda). Paleobiology 38:486–507.
1367 Bates, K. T., S. C. R. Maidment, V. Allen, and P. M. Barrett. 2012a. Computational
1368 modelling of locomotor muscle moment arms in the basal dinosaur
1369 *Lesothosaurus diagnosticus*: Assessing convergence between birds and basal
1370 ornithischians. Journal of Anatomy 220:212–232.
1371 Bauman, J. M., and Y. H. Chang. 2010. High speed x-ray video demonstrates
1372 significant skin movement errors with standard optical kinematics during rat
1373 locomotion. Journal of Neuroscience Methods 30:18–24.

1374 Bolsterlee B, H. E. Veeger , and F. C. van der Helm. 2014. Modelling clavicular and
1375 scapular kinematics: From measurement to simulation. Medical and Biological
1376 Engineering and Computing 52:283–291.
1377 Bonnan, M. F., J. L. Sandrik, T. Nishiwaki, D. R. Wilhite, R. M. Elsey, and C.
1378 Vittore. 2010. Calcified cartilage shape in archosaur long bones reflects
1379 overlying joint shape in stress-bearing elements: Implications for nonavian
1380 dinosaur locomotion. Anatomical Record 293:2044–55.
1381 Bonnan, M. F., J. Shulman, R. Varadharajan, C. Gilbert, M. Wilkes, A. Horner and E.
1382 Brainerd. 2016. Forelimb kinematics of rats using XROMM, with implications
1383 for small eutharians and their fossil relative. 11(3): e0149377.
1384 Brassey, C. A. In press. Body mass estimation in paleontology: a review of
1385 volumetric techniques. Journal of Paleontology.
1386 Brassey, C. A, S. C. R. Maidment, and P. M. Barrett. 2015. Body mass estimates of
1387 an exceptionally complete *Stegosaurus* (Ornithischia: Thyreophora): comparing
1388 volumetric and linear bivariate mass estimation methods. Biology Letters
1389 11:20140984. DOI: 10.1098/rsbl.2014.0984.
1390 Brassey, C. A., A. C. Kitchener, P. J. Withers, P. L. Manning, and W. I. Sellers. 2013.
1391 The role of cross-sectional geometry, curvature, and limb posture in maintaining
1392 equal safety factors: A computed tomography study. The Anatomical Record
1393 296:395–413.
1394 Bright, J. A. 2014. A review of paleontological finite element models and their
1395 validity. Journal of Paleontology 88:760–769.
1396 Brown, N. A. T., M. G. Pandy, C. E. Kawcak, and C. W. Mcllwraith. 2003. Force-
1397 and moment-generating capacities of muscles in the distal forelimb of the horse.
1398 Journal of Anatomy 203:101–113.

1399 Bryant, H. N., and K. L. Seymour. 1990. Observations and comments on the
1400 reliability of muscle reconstruction in fossil vertebrates. Journal of Morphology
1401 117:109–117.
1402 Bucher, I. 2004. Circle fit. Available at
1403 http://uk.mathworks.com/matlabcentral/fileexchange/5557-circle-
1404 fit/content/circfit.m (accessed 7th September 2016).
1405 Campione, N. E., and D. C. Evans. 2012. A universal scaling relationship between
1406 body mass and proximal limb bone dimensions in quadrupedal terrestrial
1407 tetrapods. BMC Biology 10:60. DOI: 10.1186/1741-7007-10-60.
1408 Carrier, D. R. 1983. Postnatal ontogeny of the musculo-skeletal system in the black-
1409 tailed jack rabbit (*Lepus californicus*). Journal of Zoology 201:27–55.
1410 Cassini, G. H., and S. F. Vizcaíno. 2012. An approach to the biomechanics of the
1411 masticatory apparatus of early Miocene (Santacrucian age) South American
1412 ungulates (Astrapotheria, Litopterna, and Notoungulata): Moment arm
1413 estimation based on 3D landmarks. Journal of Mammalian Evolution 19:9–25.
1414 Chadwick, E. K., D. Blana, A. J. van den Bogert, and R. F. Kirsch. 2009. A real-time,
1415 3-D musculoskeletal model for dynamic simulation of arm movements. IEEE
1416 Transactions on Biomedical Engineering 56:941–948.
1417 Channon, A. J., R. H. Crompton, M. M. Günther, and E. E. Vereecke. 2010. Muscle
1418 moment arms of the gibbon hind limb: implications for hylobatid locomotion.
1419 Journal of Anatomy 216:446–462.
1420 Chapman, T., F. Moiseev, V. Sholukha, S. Louryan, M. Rooze, P. Semal, and S. Van
1421 Sint Jan. 2010. Virtual reconstruction of the Neandertal lower limbs with an
1422 estimation of hamstring muscle moment arms. Comptes Rendus Palevol 9:445–
1423 454.

1424 Chinsamy-Turan, A. 2005. The Microstructure of Dinosaur Bone: Deciphering
1425 Biology with Fine-Scale Techniques. Johns Hopkins University Press,
1426 Baltimore, 216 pp.
1427 Cobley, M. J., E. J. Rayfield, and P. M. Barrett. 2013. Inter-vertebral flexibility of the
1428 ostrich neck: Implications for estimating saurpod neck flexibility. PLoS ONE
1429 8:e72187. DOI:10.1371/journal.pone.0072187.
1430 Costa, F. R., O. Rocha-Barbosa, and A. W. A. Kellner. 2013. A biomechanical
1431 approach on the optimal stance of *Anhanguera piscator* (Pterodactyloidea) and
1432 its implications for pterosaur gait on land. Historical Biology 26:582–590.
1433 Crook, T. C., S. E. Cruickshank, C. M. McGowan, N. Stubbs, A. M. Wilson, E.
1434 Hodson-Tole, and R. C. Payne. 2010. A comparison of the moment arms of
1435 pelvic limb muscles in horses bred for acceleration (Quarter Horse) and
1436 endurance (Arab). Journal of Anatomy 217:26–37.
1437 Cuff, A. R., and E. J. Rayfield. 2015. Retrodeformation and muscular reconstruction
1438 of ornithomimosaurian dinosaur crania. PeerJ 3:e1093. DOI:
1439 10.7717/peerj.1093.
1440 Curtis, N., M. E. H. Jones, A. K. Lappin, P O'Higgins, S. E. Evans, and M. J. Fagan.
1441 2010. Comparison between in vivo and theoretical bite performance: using
1442 multi-body modelling to predict muscle and bite forces in a reptile skull. Journal
1443 of Biomechanics 43:2804–2809.
1444 D'Anastasio, R., S. Wroe, C. Tuniz, L. Mancini, D. T. Cesana, D. Dreossi, M.
1445 Ravichandiran, M. Attard, W. C. H. Parr, A. Agur, and L. Capasso. 2013.
1446 Micro-biomechanics of the Kebara 2 hyoid and its implications for speech in
1447 Neanderthals. PLoS ONE 8:e82261. DOI: 10.1371/journal.pone.0082261.

1448 Damuth, J., and B. J. MacFadden. 1990. Body Size in Mammalian Paleobiology:
1449 Estimation and Biological Implications. Cambridge University Press,
1450 Cambridge, 412 pp.
1451 Delp, S. L., and W. Maloney. 1993. Effects of hip center location on the moment-
1452 generating capacity of the muscles. Journal of Biomechanics 26:485–499.
1453 Delp, S. L., J. P. Loan, M. G. Hoy, F. E. Zajac, E. L. Topp, and J. M. Rosen. 1990.
1454 An interactive graphics-based model of the lower extremity to study
1455 orthopaedic surgical procedures. IEEE Transactions on Biomedical Engineering
1456 37:757–767.
1457 Delp, S. L., F. C. Anderson, A. S. Arnold, P. Loan, A. Habib, C. T. John, E.
1458 Guendelman, and D. G. Thelen. 2007. OpenSim: Open-source software to
1459 create and analyze dynamic simulations of movement. IEEE Transactions on
1460 Biomedical Engineering 54:1940–1950.
1461 DeMar, R., and H. R. Barghusen. 1972. Mechanics and the evolution of the synapsid
1462 jaw. Evolution 26:622–637.
1463 Demes, B. 1988. Bite force, diet, and cranial morphology of fossil hominids. Journal
1464 of Human Evolution 17:657–670.
1465 Dilkes, D. W., J. R. Hutchinson, C. M. Holliday, and L. M. Witmer. 2012.
1466 Reconstructing the musculature of dinosaurs; pp. 151–190 in M. K. Brett-
1467 Surman, T. R. Holtz Jr., and J. O. Farlow (Eds.) The Complete Dinosaur.
1468 Indiana University Press, Bloomington.
1469 Domalain, M., A. Bertin, and G. Daver. In press. Was *Australopithecus afarensis* able
1470 to make the Lomekwian stone tools? Towards a realistic biomechanical
1471 simulation of hand force capacity in fossil hominins and new insights on the
1472 role of the fifth digit. Comptes Rendus Palevol.

1473 Duda, G. N., D. Brand, S. Freitag, W. Lierse, and E. Schneider. 1996. Variability of
1474 femoral muscle attachments. Journal of Biomechanics 29:1185–1190.
1475 Eckhoff, D. G., J. M. Bach, V. M. Spitzer, K. D. Reinig, M. M. Bagur, T. H. Baldini,
1476 D. Rubinstein, and S. Humphries. 2003. Three-dimensional morphology and
1477 kinematics of the distal part of the femur viewed in virtual reality, Part II.
1478 Journal Of Bone And Joint Surgery 85:97–104.
1479 Emerson, S. B., and L. Radinsky. 1980. Functional analysis of sabertooth cranial
1480 morphology. Paleobiology 6:295–312.
1481 Falkingham, P. L. 2012. Acquisition of high resolution three-dimensional models
1482 using free, open-source, photogrammetric software. Palaeontologia Electronica
1483 15:1.1T. http://palaeo-electronica.org/content/issue1-2012technical-articles/92-
1484 3d-photogrammetry
1485 Falkingham, P. L. 2014. Interpreting ecology and behaviour from the vertebrate fossil
1486 track record. Journal of Zoology 292:222–228.
1487 Favre, P., M. D. Loeb, N. Helmy, and C. Gerber. 2008. Latissimus dorsi transfer to
1488 restore external rotation with reverse shoulder arthroplasty: A Biomechanical
1489 Study. Journal of Shoulder and Elbow Surgery 17:650–658.
1490 Fisher, H. I. 1945. Locomotion in the Fossil Vulture *Teratornis*. American Midland
1491 Naturalist 33:725–742.
1492 Fox, R. C. 1964. The adductor muscles of the jaw in some primitive reptiles.
1493 University of Kansas Public Museum of Natural History 12:657–680.
1494 Fujiwara, S., and J. R. Hutchinson. 2012. Elbow joint adductor moment arm as an
1495 indicator of forelimb posture in extinct quadrupedal tetrapods. Proceedings of
1496 the Royal Society B: Biological Sciences 279:2561–2570.

1497 Gans, C., and F. De Vree. 1987. Functional bases for fiber length and angulation in
1498 muscle. Journal of Morphology 192:63–85.
1499 Garner, B. A., and M. G. Pandy. 2000. The obstacle-set method for representing
1500 muscle paths in musculoskeletal models. Computer Methods in Biomechanics
1501 and Biomedical Engineering 3:1–30.
1502 Gatti, C. J., C. Dickerson, E. K. Chadwick, A. G. Mell, and R. E. Hughes. 2007.
1503 Comparison of model-predicted and measured moment arms for the rotator cuff
1504 muscles. Clinical Biomechanics 22:639–644.
1505 Gill, P. G., M. A. Purnell, N. Crumpton, K. Robson Brown, N. J. Gostling, M.
1506 Stampanoni, and E. J. Rayfield. 2014. Dietary specializations and diversity in
1507 feeding ecology of the earliest stem mammals. Nature 512:303–305.
1508 Gregory, R. D. 2006. Classical Mechanics. Cambridge University Press, Cambridge,
1509 608 pp.
1510 Gröning, F., M. E. H. Jones, N. Curtis, A. Herrel, P. O'Higgins, S. E. Evans, and M. J.
1511 Fagan. 2013. The importance of accurate muscle modelling for biomechanical
1512 analyses: a case study with a lizard skull. Journal of The Royal Society Interface
1513 10:20130216. DOI: 10.1098/rsif.2013.0216.
1514 Hartstone-Rose, A., J. M. G. Perry, and C. J. Morrow. 2012. Bite force estimation and
1515 the fiber architecture of felid masticatory muscles. Anatomical Record
1516 295:1336–1351.
1517 Hatala, K. G., R. G. Wunderlich, H. L. Dingwall, and B. G. Richmond. 2016.
1518 Interpreting locomotor biomechanics from the morphology of human footprints.
1519 Journal of Human Evolution 90:38–48.
1520 Hieronymus, T. L. 2006. Quantitative microanatomy of jaw muscle attachment in
1521 extant diapsids. Journal of Morphology 267:954–967.

1522 Henderson, D. M. 2006. Burly gaits: Centers of mass, stability, and the trackways of
1523 sauropod dinosaurs. Journal of Vertebrate Paleontology 26:907–921.
1524 Herzog, W., and L. J. Read. 1993. Lines of action and moment arms of the major
1525 force-carrying structures crossing the human knee joint. Journal of Anatomy
1526 182:213–230.
1527 Hicks, J. L., T. K. Uchida, A. Seth, A. Rajagopal, and S. L. Delp. 2014. Is my model
1528 good enough? Best practices for verification and validation of musculoskeletal
1529 models and simulations of human movement. Journal of Biomechanical
1530 Engineering 137:020905. DOI: 10.1115/1.4029304.
1531 Holliday, C. M. 2009. New insights into dinosaur jaw muscle anatomy. Anatomical
1532 Record 292:1246–1265.
1533 Holliday, C. M., R. C. Ridgley, J. C. Sedlmayr, and L. M. Witmer. 2010.
1534 Cartilaginous epiphyses in extant archosaurs and their implications for
1535 reconstructing limb function in dinosaurs. PLoS ONE 5:e13120. DOI:
1536 10.1371/journal.pone.0013120.
1537 Holokwa, N. B., and M. C. O'Neill. 2013. Three-dimensional moment arms and
1538 architecture of chimpazee (*Pan troglodytes*) leg musculature. Journal of
1539 Anatomy 223:610–628.
1540 Holzbaur, K. R. S., W. M. Murray, and S. L. Delp. 2005. A model of the upper
1541 extremity for simulating musculoskeletal surgery and analyzing neuromuscular
1542 control. Annals of Biomedical Engineering 33:829–840.
1543 Hughes, R. E., G. Niebur, J. Liu, and K. N. An. 1998. Comparison of two methods for
1544 computing abduction moment arms of the rotator cuff. Journal of Biomechanics
1545 31:157–160.

1546 Hutchinson, J. R. 2001a. The evoluton of femoral osteology and soft tissue on the line
1547 to extant birds. Zoological Journal of the Linnean Society 131:169–197.
1548 Hutchinson, J. R. 2001b. The evoluton of pelvic osteology and soft tissue on the line
1549 to extant birds. Zoological Journal of the Linnean Society 131:123–168.
1550 Hutchinson, J. R. 2002. The evolution of hindlimb tendons and muscles on the line to
1551 crown-group birds. Comparative Biochemistry and Physiology Part A
1552 133:1051–1086.
1553 Hutchinson, J. R. 2011. On the inference of function from structure using
1554 biomechanical modelling and simulation of extinct organisms. Biology Letters
1555 23:115–118.
1556 Hutchinson, J. R., and M. T. Carrano. 2002. Pelvic and hindlimb musculature of
1557 *Tyrannosaurus rex* (Dinosauria: Theropoda). Journal of Morphology 253:207–
1558 228.
1559 Hutchinson, J. R., F. C. Anderson, S. S. Blemker, and S. L. Delp. 2005. Analysis of
1560 hindlimb muscle moment arms in *Tyrannosaurus rex* using a three-dimensional
1561 musculoskeletal computer model: Implications for stance, gait, and speed.
1562 Paleobiology 31:676–701.
1563 Hutchinson, J. R., J. W. Rankin, J. Rubenson, K. H. Rosenbluth, R. A. Siston , and S.
1564 L. Delp. 2015. Musculoskeletal modeling of an ostrich (*Struthio camelus*) pelvic
1565 limb: Influence of limb orientation on muscular capacity during locomotion.
1566 PeerJ 3:e1001. DOI: 10.7717/peerj.1001.
1567 Hutson, J. D., and K. N. Hutson. 2012. A test of the validity of range of motion
1568 studies of fossil archosaur elbow mobility using repeated-measures analysis and
1569 the extant phylogenetic bracket. Journal of Experimental Biology 215:2030–
1570 2038.

1571 Hutson, J. D., and K. N. Hutson. 2013. Using the American alligator and a repeated-
1572 measures design to place constraints on in vivo shoulder joint range of motion
1573 in dinosaurs and other fossil archosaurs. Journal of Experimental Biology
1574 216:275–84.
1575 Inman, V. T., J. B. D. Saunders, L. C. Abbott. 1944. Observations on the function of
1576 the shoulder joint. *The Journal of Bone and Joint Surgery.* 26:1-30.
1577 Iuliis, G. de, M. S. Bargo, and S. F. Vizcaino. 2001. Variation in skull morphology
1578 and mastication in the fossil giant armadillos *Pampatherium spp*. and allied
1579 genera (Mammalia: Xenarthra: Pampatheriidae), with comments on their
1580 systematics and distribution. Journal of Vertebrate Paleontology 20:743–754.
1581 Iwaki, H., V. Pinskerova, and M. A. R. Freeman. 2002. Tibiofemoral movement 1:
1582 The shapes and the unloaded cadaver knee. The Journal of Bone and Joint
1583 Surgery 82:108–119.
1584 Johnson, R. E., and J. H. Ostrom. 1995. The forelimb of *Torosaurus* and an analysis
1585 of the posture and gait of ceratopsian dinosaurs; pp. 205–218 in J. J. Thomason
1586 (Ed.), Functional Morphology in Vertebrate Paleontology. Cambridge
1587 University Press, Cambridge.
1588 Johnson, W. L. 2009. Musculoskeletal model of the rat hindlimb. Simtk.org.
1589 Available at: https://simtk.org/home/rat_hlimb_model.
1590 Johnson, W. L., D. L. Jindrich, R. R. Roy, and V. R. Edgerton. 2008. A three-
1591 dimensional model of the rat hindlimb: Musculoskeletal geometry and muscle
1592 moment arms. Journal of Biomechanics 41:610–619.
1593 Jones, M. E. H., P. O'Higgins, M. J. Fagan, S. E. Evans, and N. Curtis. 2012. Shearing
1594 mechanics and the influence of a flexible symphysis during oral food processing

in *Sphenodon* (Lepidosauria: Rhynchocephalia). Anatomical Record 295:1075–1091.

Juul-Kristensen, B., F. Bojsen-Møller, E. Holst, and C. Ekdahl. 2000. Comparison of muscle sizes and moment arms of two rotator cuff muscles measured by ultrasonography and magnetic resonance imaging. European Journal of Ultrasound 11:161–173.

Kappelman, J. 1988. Morphology and locomotor adaptations of the bovid femur in relation to habitat. Journal of Morphology 198:119–130.

Kargo, W. J., and L. C. Rome. 2002. Functional morphology of proximal hindlimb muscles in the frog *Rana pipiens*. Journal of Experimental Biology 205:1987–2004.

Karlsson, D., and B. Peterson. 1992. Towards a model for force predictions in the human shoulder. Journal of Biomechanics 25:189–199.

Klein Horsman, M. D., H. F. Koopman, F. C. van der Helm, L. P. Prosé, and H. E. Veeger. 2007. Morphological muscle and joint parameters for musculoskeletal modelling of the lower extremity. Clinical Biomechanics 22:239–247.

Kumar, S. 1988. Moment arms of spinal musculature determined from CT scans. Clinical Biomechanics 3:137–44.

Lautenschlager, S. 2016. Reconstructing the past: methods and techniques for the digital restoration of fossils. Royal Society Open Science 3:160342. DOI: 10.1098/rsos.160342.

Lautenschlager, S., C. A. Brassey, D. J. Button, and P. M. Barrett. 2016. Decoupled form and function in disparate herbivorous dinosaur clades. Scientific Reports 6:26495. DOI: 10.1038/srep26495.

1619 Lautenschlager, S., L. M. Witmer, P. Altangerel, L. E. Zanno, and E. J. Rayfield.
1620 2014. Cranial anatomy of *Erlikosaurus andrewsi* (Dinosauria, Therizinosauria):
1621 New insights based on digital reconstruction. Journal of Vertebrate
1622 Paleontology 34:1263–1291.
1623 Lerner, Z. F., B. C. Gadomski, A. K. Ipson, K. K. Haussler, C. M. Puttlitz, and R. C.
1624 Browning. 2015. Modulating tibiofemoral contact force in the sheep hind limb
1625 via treadmill walking: Predictions from an OpenSim musculoskeletal model.
1626 Journal of Orthopaedic Research 33:1128–1133.
1627 Maganaris, C. N. 2004. Imaging-based estimates of moment arm length in intact
1628 human muscle-tendons. European Journal of Applied Physiology 91:130–139.
1629 Maidment, S. C. R., and P. M. Barrett. 2011. The locomotor musculature of basal
1630 ornithischian dinosaurs. Journal of Vertebrate Paleontology 31:1265–1291.
1631 Maidment, S. C. R., and P. M. Barrett. 2012. Does morphological convergence imply
1632 functional similarity? A test using the evolution of quadrupedalism in
1633 ornithischian dinosaurs. Proceedings of the Royal Society B 279:3765–3771.
1634 Maidment, S. C. R., K. T. Bates, and P. M. Barrett. 2014b. Three-dimensional
1635 computational modeling of pelvic locomotor muscle moment arms in
1636 *Edmontosaurus* (Dinosauria, Hadrosauridae) and comparisons with other
1637 archosaurus; pp. 443–448 in D. A. Eberth and D. C. Evans (Eds.), Hadrosaurs.
1638 Indiana University Press, Bloomington.
1639 Maidment, S. C. R., C. A. Brassey, and P. M. Barrett. 2015. The postcranial skeleton
1640 of an exceptionally complete individual of the plated dinosaur *Stegosaurus*
1641 *stenops* (Dinosauria: Thyreophora) from the Upper Jurassic Morrison Formation
1642 of Wyoming, U.S.A. PLoS ONE 10:e0138352. DOI:
1643 10.1371/journal.pone.0138352.

1644 Maidment, S. C. R., K. T. Bates, P. L. Falkingham, C. VanBuren, V. Arbour, and P.
1645 M. Barrett. 2014a. Locomotion in ornithischian dinosaurs: An assessment using
1646 three-dimensional computational modelling. Biological Reviews 89:588–617.
1647 Malda, J., J. C. de Grauw, K. E. Benders, M. J. Kik, C. H. van de Lest, L. B.
1648 Creemers, W. J. Dhert, and P. R. van Weeren. 2013. Of Mice, Men and
1649 Elephants: The relation between articular cartilage thickness and body mass.
1650 PLoS ONE 8:e57683. DOI: 10.1371/journal.pone.0057683.
1651 Mallison, H. 2010a. CAD assessment of the posture and range of motion of
1652 *Kentrosaurus aethiopicus* (Hennig 1915). Swiss Journal of Geoscience
1653 103:211–233.
1654 Mallison, H. 2010b. The Digital *Plateosaurus* II: An assessment of the range of
1655 motion of the limbs and vertebral column and of previous reconstructions using
1656 a digital skeletal mount. Acta Palaeontologica Polonica 55:433–458.
1657 Mallison, H., and O. Wings. 2014. Photogrammetry in Paleontology – A Practical
1658 Guide. Journal of Paleontological Techniques 12:1–31.
1659 Martín-Serra, A., B. Figueirido, and P. Palmqvist. 2014. A three-dimensional analysis
1660 of morphological evolution and locomotor performance of the carnivoran
1661 forelimb. PLoS ONE 9:e85574. DOI: 10.1371/journal.pone.0085574.
1662 Maynard Smith, J., and R. J. G. Savage. 1956. Some locomotory adaptations in
1663 mammals. Zoological Journal of the Linnean Society 42:603–22.
1664 McGowan, C. 1979. The hind limb musculature of the Brown kiwi, *Apteryx australis*
1665 *mantelli*. Journal of Morphology 160:33–74.
1666 McHenry, H. M. 1975. Biomechanical interpretation of the early hominid hip. Journal
1667 of Human Evolution 4:343–355.

1668 McHenry, C. R., S. Wroe, P. D. Clausen, K. Moreno, and E. Cunningham. 2007.
1669 Supermodeled sabercat, predatory behaviour in *Smilodon fatalis* revealed by
1670 high-resolution 3D computer simulation. Proceedings of the National Academy
1671 of Sciences of the United States of America 104:16010–16015.
1672 McNamara, M., P. J. Orr, S. L. Kearns, L. Alcalá, P. Anadón, and E. Peñalver-Mollá.
1673 2010. Organic preservation of fossil musculature with ultracellular detail.
1674 Proceedings of the Royal Society B: Biological Sciences 277:423–427.
1675 Meers, M. B. 2003. Crocodylian forelimb musculature and its relevance to
1676 Archosauria. Anatomical Record 274:891–916.
1677 Miller, L. H. 1915. A walking eagle from Rancho La Brea. The Condor 17:179–181.
1678 Montani, R. 1997. New technique for retrodeforming tectonically deformed fossils,
1679 with am example for ichthyosaurian specimens. Lethaia 30:221–228.
1680 Morton, D. J. 1924. Evolution of the human foot II. American Journal of Physical
1681 Anthropology 7:1–52.
1682 Murray, W. M., T. S. Buchanan, and S. L. Delp. 2002. Scaling of peak moment arms
1683 of elbow muscles with upper extremity bone dimensions. Journal of
1684 Biomechanics 35:19–26.
1685 Murray, W. M., A. S. Arnold, S. Salinas, M. M. Durbhakula, T. S. Buchanan, and S.
1686 L. Delp. 1998. Building biomechanical models based on medical image data: an
1687 assessment of model accuracy; pp. 539–549 in W. M. Wells, A. Colchester, and
1688 S. L. Delp (Eds.), Medical Image Computing and Computer-Assisted
1689 Intervention. Springerverlag, Berlin and Heidelberg.
1690 Nagano, A., B. R. Umberger, M. W. Marzke, K. G. M. Gerritsen. 2005.
1691 Neuromusculoskeletal computer modelling and simulation of upright, straight-

1692 legged, bipedal locomotion of *Australopithecus afarensis.* American Journal of
1693 Physical Anthropology 126:2-13.
1694 Neenan, J. M., M. Ruta, J. A. Clack, and E. J. Rayfield. 2014. Feeding biomechanics
1695 in *Acanthostega* and across the fish-tetrapod transition. Proceedings of the
1696 Royal Society B: Biological Sciences 281:20132689. DOI:
1697 10.1098/rspb.2013.2689.
1698 Noble, H. 1973. Comparative functional anatomy of temporomandibular joint. Oral
1699 Sciences Reviews 2:3–28.
1700 O'Neill, M. C., L. F. Lee, S. G. Larson, B. Demes, J. T. Stern, and B. R. Umberger.
1701 2013. A three-dimensional musculoskeletal model of the chimpanzee (*Pan*
1702 *troglodytes*) pelvis and hind limb. Journal of Experimental Biology 216:3709–
1703 23.
1704 Ogihara, N., H. Makishima, S. Aoi, Y. Sugimoto, K. Tsuchiya, and M. Nakatsukasa.
1705 2009. Development of an anatomically based whole-body musculoskeletal
1706 model of the Japanese Macaque (*Macaca fuscata*). American Journal of
1707 Physical Anthropology 139:323–338.
1708 Otis, J. C., C. C. Jiang, T. L. Wickiewicz, M. G. Peterson, R. F. Warren, and T. J.
1709 Santner. 1994. Changes in the moment arms of the rotator cuff and deltoid
1710 muscles with abduction and rotation. The Journal of Bone and Joint Surgery
1711 76:667–76.
1712 Payne, R. C., R. H. Crompton, K. Isler, R. Savage, E. E. Vereecke, M. M. Günther, S.
1713 K. S. Thorpe, and K. D' Août. 2006. Morphological analysis of the hindlimb in
1714 apes and humans. II. Moment arms. Journal of Anatomy 208:725–742.

1715 Petermann, H., and M. Sander. 2013. Histological evidence for muscle insertion in
1716 extant amniote femora: Implications for muscle reconstructions. Journal of
1717 Anatomy 222:419–436.
1718 Peters, S., and J. Hsu. 2014. Comparison of rigid body dynamic simulators for robotic
1719 simulation in gazebo, in Open Source Robotics Foundation. Available from:
1720 http://www.osrfoundation.org/wordpress2/wp-
1721 content/uploads/2015/04/roscon2014_scpeters.pdf (accessed 8th September
1722 2016).
1723 Piazza, S. J., Pand . R. Cavanagh. 2000. Measurement of the screw-home motion of
1724 the knee is sensitive to errors in axis alignment. Journal of Biomechanics
1725 33:1029–1034.
1726 Pierce, S. E., J. A. Clack, and J. R. Hutchinson. 2012. Three-dimensional limb joint
1727 mobility in the early tetrapod *Ichthyostega*. Nature 486:523–526.
1728 Pillet, H., M. Sangeux, J. Hausselle, R. E. Rachkidi, and W. Skalli. 2014. A reference
1729 method for the evaluation of femoral head joint center location technique based
1730 on external markers. Gait and Posture 39:655–658.
1731 R Core Team 2016. R: A Language and Environment for Statistical Computing. R
1732 Foundation for Statistical Computing. Vienna, Austria. http://www.R-
1733 project.org.
1734 Ravosa, M. 1996. Jaw morphology and function in living and fossil old world
1735 monkeys. International Journal of Primatology 17:909–32.
1736 Ren, L., M. Butler, C. Miller, H. Paxton, D. Schwerda, M. S. Fischer, and J. R.
1737 Hutchinson. 2008. The movements of limb segments and joints during
1738 locomotion in African and Asian elephants. Journal of Experimental Biology
1739 211:2735–2751.

1740 Sammarco, G. J., A. H. Burstein, and V. H. Frankel. 1973. Biomechanics of the ankle:
1741 A kinematic study. The Orthopedic Clinics of North America 4:75–96.
1742 Schaffelhofer, S., S. Sartori, H. Scherberger, and D. Farina. 2015. Musculoskeletal
1743 representation of a large repertoire of hand grasping actions in primates. IEEE
1744 Transactions on Neural Systems and Rehabilitation Engineering A 23:210–220.
1745 Sellers, W. I. 2014. GaitSym 2014 Config Reference Manual. Available from:
1746 http://www.animalsimulation.org/page3/page7/page7.html.
1747 Sellers, W. I., and P. L. Manning. 2007. Estimating dinosaur maximum running
1748 speeds using evolutionary robotics. Proceedings of the Royal Society B:
1749 Biological Sciences 274:2711–2716.
1750 Sellers, W. I., G. M. Cain, W. Wang, and R. H. Crompton. 2005. Stride lengths, speed
1751 and energy costs in walking of *Australopithecus afarensis*: Using evolutionary
1752 robotics to predict locomotion of early human ancestors. Journal of the Royal
1753 Society Interface 2:431–441.
1754 Sellers, W.I., L. Margetts, K. T. Bates, and A. T. Chamberlain. 2013a. Exploring
1755 diagonal gait using a forward dynamic three-dimensional chimpanzee
1756 simulation. Folia Primatologica 84:180–200.
1757 Sellers, W. I., L. Margetts, R. A. Coria, and P. L. Manning. 2013b. March of the
1758 titans: The locomotor capabilities of sauropod dinosaurs. PLoS ONE 8:e78733.
1759 DOI: 10.1371/journal.pone.0078733.
1760 Sellers, W. I., T. C. Pataky, P. Caravaggi, and R. H. Crompton. 2010. Evolutionary
1761 robotic approaches in primate gait analysis. International Journal of Primatology
1762 31:321–338.
1763 Sellers, W. I., P. L. Manning, T. Lyson, K. Stevens, and L. Margetts. 2009. Virtual
1764 palaeontology: Gait reconstruction of extinct vertebrates using high

1765 performance computing. Palaeontologia Electronica 12:13A. http://palaeo-
1766 electronica.org/2009_3/180/index.html
1767 Senter, P., and J. H. Robins. 2005. Range of motion in the forelimb of the theropod
1768 dinosaur *Acrocanthosaurus atokensis*, and implications for predatory behaviour.
1769 Journal of Zoology 266:307–318.
1770 Sholukha, V., B. Bonnechere, P. Salvia, F. Moiseev, M. Rooze, and S. Van Sint Jan.
1771 2013. Model-based approach for human kinematics reconstruction from
1772 markerless and marker-based motion analysis systems. Journal of Biomechanics
1773 46:2363–2371.
1774 Simpson, G. G., and H. O. Elftman. 1928. Hind limb musculature and habits of a
1775 Paleocene multituberculate. American Museum Novitates 333: 1-19.
1776 Singleton, M. 2015. Functional geometric morphometric analysis of masticatory
1777 system ontogeny in papionin primates. Anatomical Record 298:48–63.
1778 Smith, K. K., and K. H. Redford. 1990. The anatomy and function of the feeding
1779 apparatus in two armadillos (Dasypoda): Anatomy is not destiny. Journal of
1780 Zoology 222:27–47.
1781 Smith, N. C., R. C. Payne, K. J. Jespers, and A. M. Wilson. 2007. Muscle moment
1782 arms of pelvic limb muscles of the ostrich (*Struthio camelus)*. Journal of
1783 Anatomy 211:313–24.
1784 Snively, E., J. M. Fahlke, and R. C. Welsh. 2015. Bone-breaking bite force of
1785 *Basilosaurus isis* (Mammalia, Cetacea) from the late Eocene of Egypt estimated
1786 by finite element analysis. PLoS ONE 10:e0118380. DOI:
1787 10.1371/journal.pone.0118380.
1788 Snively, E., J. R. Cotton, R. Ridgley, and L. M. Witmer. 2013. Multibody dynamics
1789 model of head and neck function in *Allosaurus* (Dinosauria, Theropoda).

1790 Palaeontologia Electronica 16(2):11A. http://palaeo-
1791 electronica.org/content/2013/389-allosaurus-feeding
1792 Sommer, H. J., N. R. Miller, and G. J. Pijanowski. 1982. Three-dimensional
1793 osteometric scaling and normative modeling of skeletal segments. Journal of
1794 Biomechanics 15:171–180.
1795 Spoor, C. W., and J. L. van Leeuwen. 1992. Knee muscle moment arms from MRI
1796 and from tendon travel. Journal of Biomechanics 25:201–206.
1797 Steele, K. M., M. S. Demers, M. H. Schwartz, and S. L. Delp. 2012. Compressive
1798 tibiofemoral force during crouch gait. Gait and Posture 35:556–60.
1799 Stern, J. T. 1974. Computer modelling of gross muscle dynamics. Journal of
1800 Biomechanics 7:411–428.
1801 Sustaita, D., S. M. Gatesy, and T. J. Roberts. 2015. Reconciling variation in moment
1802 arms and measurement techniques for Emu toe joints [abstract no 104.2].
1803 Society for Integrative and Comparative Biology Annual Meeting 2015.
1804 Sutton, M., I. Rahman, and R. Garwood. 2014. Techniques for Virtual Palaeontology.
1805 Wiley Blackwell, Chichester, 208 pp.
1806 Tambussi, C. P., R. D. Mendoza, F. J. Degrange, and M. B. Picasso. 2012. Flexibility
1807 along the neck of the neogene terror bird *Andalgalornis steulleti* (Aves
1808 Phorusrhacidae). PLoS ONE 7:e37701. DOI: 10.1371/journal.pone.0037701.
1809 Taylor, G. K., and A. L. R. Thomas. 2014. Evolutionary Biomechanics: Selection,
1810 Phylogeny and Constraint. Oxford University Press, Oxford, 176 pp.
1811 Taylor, M. P., and M. J. Wedel. 2013. The effect of intervertebral cartilage on neutral
1812 posture and range of motion in the necks of sauropod dinosaurs. PLoS ONE
1813 8:e78214. DOI: 10.1371/journal.pone.0078214.

1814 Taylor, P., and P. Senter. 2010. Comparison of forelimb function between
1815 *Deinonychus* and *Bambiraptor* (Theropoda: Dromaeosauridae). Journal of
1816 Vertebrate Paleontology 26:897–906.
1817 Terhune, C. E., J. Iriarte-Diaz, A. B. Taylor, and C. F. Ross. 2011. The instantaneous
1818 center of rotation of the mandible in nonhuman primates. Integrative and
1819 Comparative Biology 51:320–332.
1820 Van der Helm, F. C. T., and R. Veenbaas. 1991. Modelling the mechanical effect of
1821 muscles with large attachment sites: Application to the shoulder mechanism.
1822 Journal of Biomechanics 24:1151–1163.
1823 Van der Helm, F. C. T., H. E. J. Veeger, G. M. Pronk, L. H. V. Van der Woude, and
1824 R. H. Rozendal. 1992. Geometry parameters for musculoskeletal modelling of
1825 the shoulder system. Journal of Biomechanics 25:129–144.
1826 Veeger, H. E. J. 2000. The position of the rotation center of the glenohumeral joint.
1827 Journal of Biomechanics 33:1711–1715.
1828 Veeger, H. E. J., and F. C. T. van der Helm. 2007. Shoulder function: The perfect
1829 compromise between mobility and stability. Journal of Biomechanics 40:2119–
1830 2129.
1831 Vizcaíno, S. F., and G. de Iuliis. 2003. Evidence for advanced carnivory in fossil
1832 armadillos (Mammalia: Xenarthra: Dasypodidae). Journal of Vertebrate
1833 Paleontology 29:123–138.
1834 Watson, P. J., F. Gröning, N. Curtis, L. C. Fitton, A. Herrel, S. W. McCormack, and
1835 M. J. Fagan. 2014. Masticatory biomechanics in the rabbit: A multi-body
1836 dynamics analysis. Journal of The Royal Society Interface 11:20140564. DOI:
1837 10.1098/rsif.2014.0564.

1838 Webb, J. D., S. S. Blemker, and S. L. Delp. 2012. 3D finite element models of
1839 shoulder muscles for computing lines of actions and moment arms. Computer
1840 Methods in Biomechanics and Biomedical Engineering 17:829–837.
1841 Wehner, T., U. Wolfram, T. Henzler, F. Niemeyer, L. Claes, and U. Simon. 2010.
1842 Internal forces and moments in the femur of the rat during gait. Journal of
1843 Biomechanics 43:2473–2479.
1844 Williams, S. B., A. M. Wilson, L. Rhodes, J. Andrews, and R. C. Payne. 2008.
1845 Functional anatomy and muscle moment arms of the pelvic limb of an elite
1846 sprinting athlete: The racing greyhound (*Canis familiaris*). Journal of Anatomy
1847 213:361–72.
1848 Witmer, L. M. 1995a. The extant phylogenetic bracket and the importance of
1849 reconstructing soft tissues in fossils; pp. 19–33 in Thomason, J. J. (Ed.),
1850 Functional Morphology in Vertebrate Paleontology. Cambridge University
1851 Press, Cambridge.
1852 Witmer, L. M. 1995b. Homology of facial structures in extant archosaurs (birds and
1853 crocodilians), with special reference to paranasal pneumaticity and nasal
1854 conchae. Journal of Morphology 255:269–327.
1855 Witzmann, F., and R. R. Schoch. 2013. Reconstruction of cranial and hyobranchial
1856 muscles in the Triassic temnospondyl *Gerrothorax* provides evidence for
1857 akinetic suction feeding. Journal of Morphology 274:525–42.
1858 Wroe, S., K. Moreno, P. Clausen, C. McHenry, and D. Curnoe. 2007. High-resolution
1859 three-dimensional computer simulation of hominid cranial mechanics.
1860 Anatomical Record 290:1248–1255.
1861 Wroe, S., U. Chamoli, W. C. Parr, P. Clausen, R. Ridgely, and L. M. Witmer. 2013.
1862 Comparative biomechanical modeling of metatherian and placental saber-

1863 tooths: A different kind of bite for an extreme pouched predator. PLoS ONE
1864 8:8–16. DOI: 10.1371/journal.pone.0066888.
1865 Young, J. W. 2005. Ontogeny of muscle mechanical advantage in capuchin monkeys
1866 (*Cebus albifrons* and *Cebus apella*). Journal of Zoology 267:351–362.
1867 Zumwalt, A. 2006. The effect of endurance exercise on the morphology of muscle
1868 attachment sites. Journal of Experimental Biology 209:444–54.
1869
1870 Submitted November 23, 2016; accepted Month DD, YYYY.
1871

1872

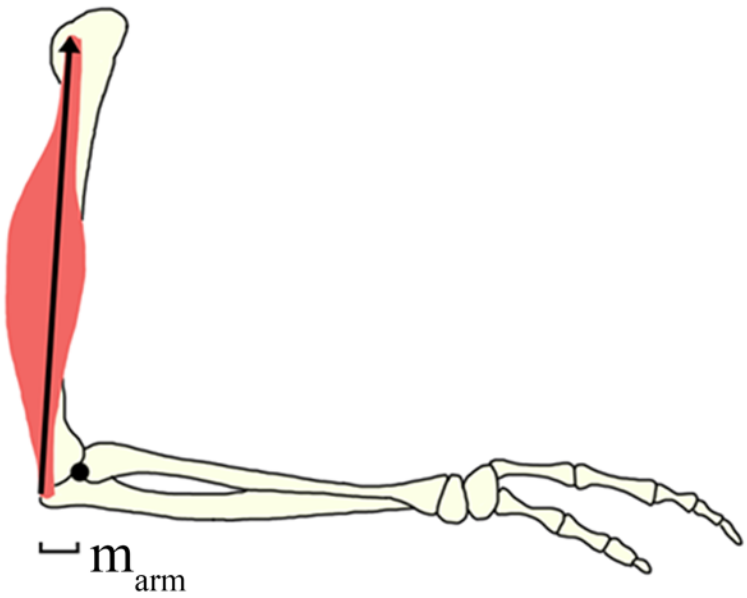

FIGURE 1. Schematic of human M. triceps moment arm calculation illustrating the 2D origin-insertion method. Moment arm is calculated as the perpendicular distance from the muscle line of action to the joint center [Intended for column width].

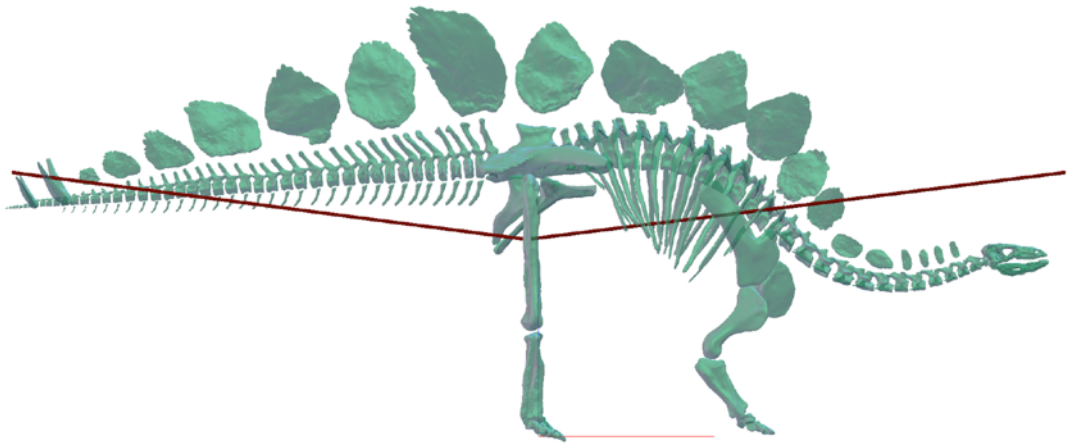

FIGURE 2. A 3D articulated model of *Stegosaurus stenops* in right lateral view. Red lines represent a pair of antagonistic 'driver' muscles attaching to the midshaft of the anterior and posterior surface of the femoral midshaft, used for driving the position of the femur to extreme hip flexion and hip extension respectively. [Intended for column width].

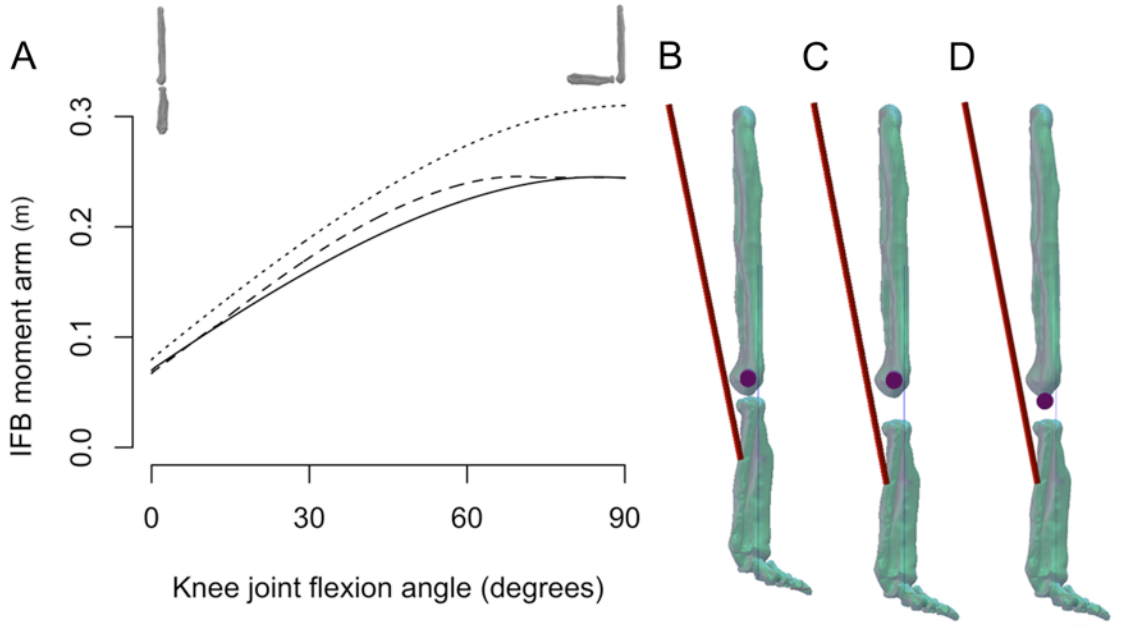

FIGURE 3. Quantifying the effect of articular cartilage on M. iliofibularis (IFB) moment arms measured around the knee. **A**, solid line represents IFB moment arm without articular cartilage separating the distal condyles of the femur and proximal surface of the tibia, as illustrated in **B**; dotted line represents moment arm of IFB calculated with an additional 10% of length added to the femur and tibia (of which half is located at the knee) while joint center remains unchanged, as illustrated in **C**; dashed line represented IFB moment arm calculated with 10% additional cartilage and joint center shifted distally, as illustrated in **D**. [Intended for 2/3 page width].

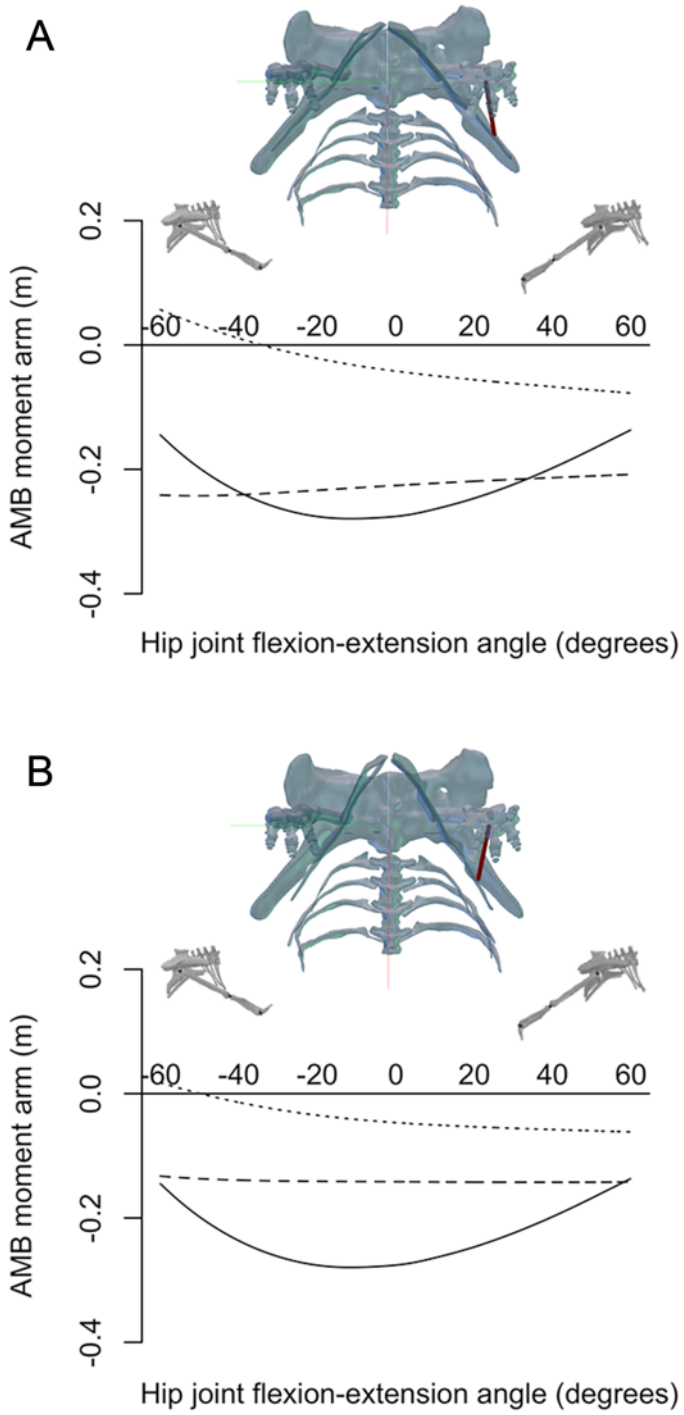

1895

1896 FIGURE 4. Quantifying the effect of the positioning of the pubis on M. ambiens

1897 (AMB) moment arms measured around the hip. Positive values for moment arms

1898 imply hip extension, hip adduction, and lateral femoral rotation for FlexExt, AbdAdd,

1899 and LAR respectively. Solid lines represent AMB FlexExt, dashed lines represent

AMB AbdAdd, and dotted lines represent AMB LAR. Path of AMB marked in red on skeletal model. **A**, illustrates the pubis orientated parallel to the iliac blades; **B**, illustrates pubis rotated medially from this position. [Intended for column width].

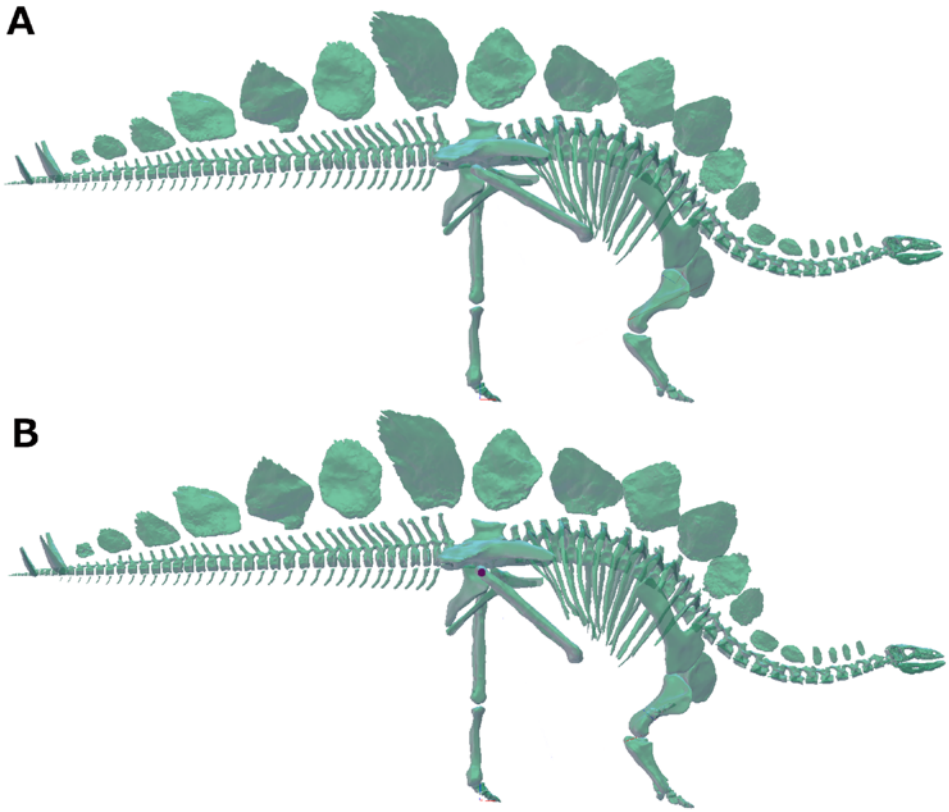

FIGURE 5. Determining range of motion in the hip. **A**, hip flexion of 60° results in collision between the femur and last dorsal ribs whereas; **B**, hip flexion of 50° could have been achieved without contact between the hind limb and torso. This reflects the bony limits to range of motion, whilst the physiological limb postures achievable may have been more limited. [Intended for column width].

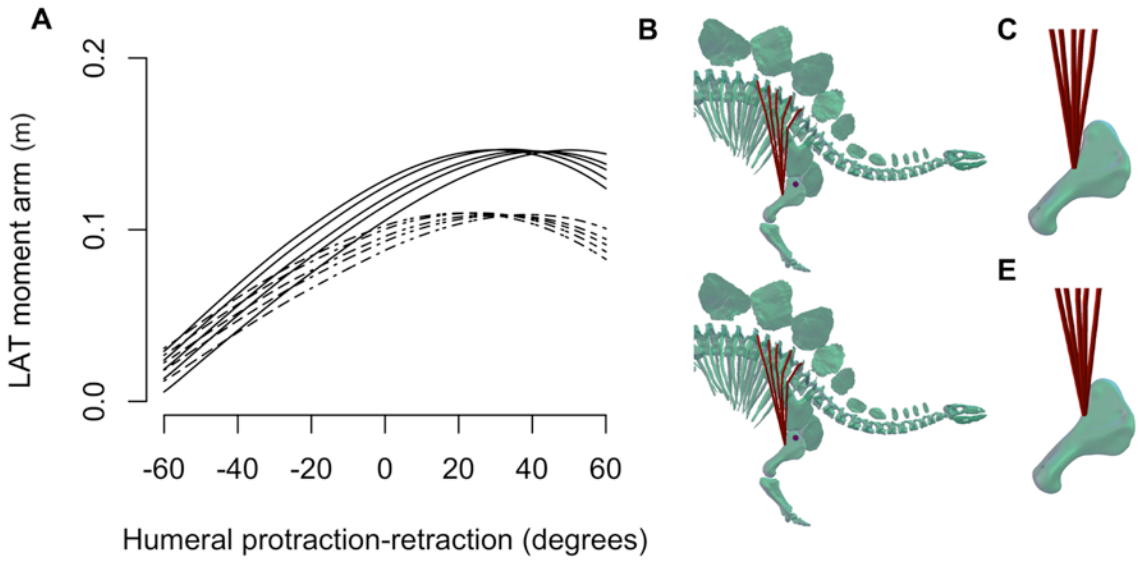

1911

1912

1913 FIGURE 6. **A**, variation in M. latissimus dorsi (LAT) moment arm with humeral

1914 protraction-retraction for five lines of action. A negative joint angle is protraction,

1915 while a positive joint angle is retraction. A positive moment arm indicates shoulder

1916 retractor leverage. Solid lines, centroidal insertion of LAT on posterior surface of the

1917 humerus, as illustrated in **B–C**. Dashed lines, LAT insertion shifted to most proximal

1918 extent, as illustrated in **D–E**. [Intended for 2/3 page width].

1919

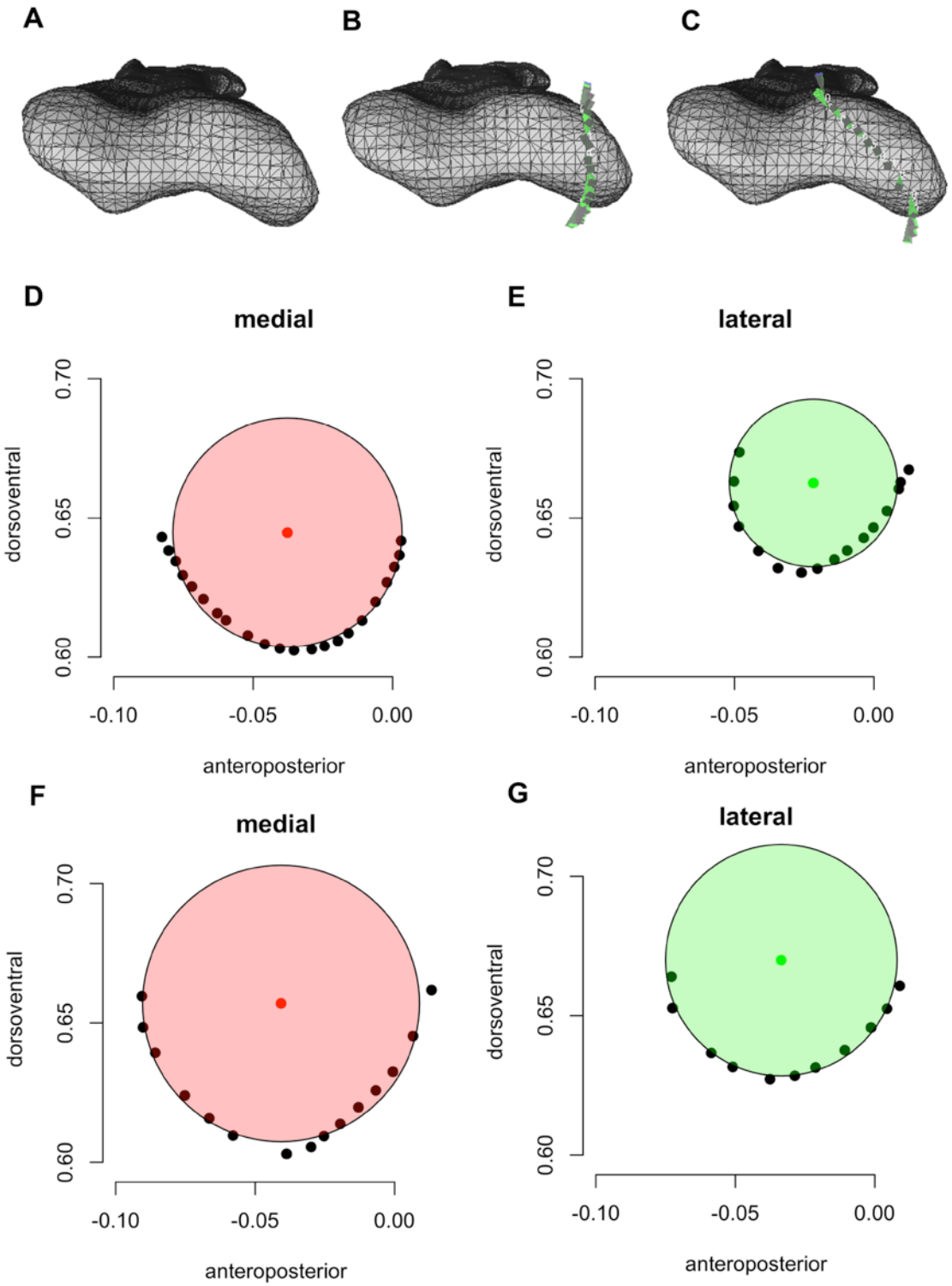

1920

1921

1922 FIGURE 7. The calculation of knee joint center via circle fitting to the medial and

1923 lateral condyles. **A**, ventral view of the distal femoral condyles displaying taphonomic

1924 distortion; **B**, markers indicate the vertices at which coordinate data was collected for

the medial condyle along a line running anteroposteriorly; **C**, coordinate data collected from vertices located along a line describing the long-axis of the distorted medial condyle; **D–E**, circles fitted to the medial and lateral condyles respectively, based on vertices sampled in a strict anteroposterior plane; **F–G**, circles fitted to medial and lateral condyles when accounting for warping of the condylar long axis. Colored dots indicate centroid of circle. [Intended for 2/3 page width].

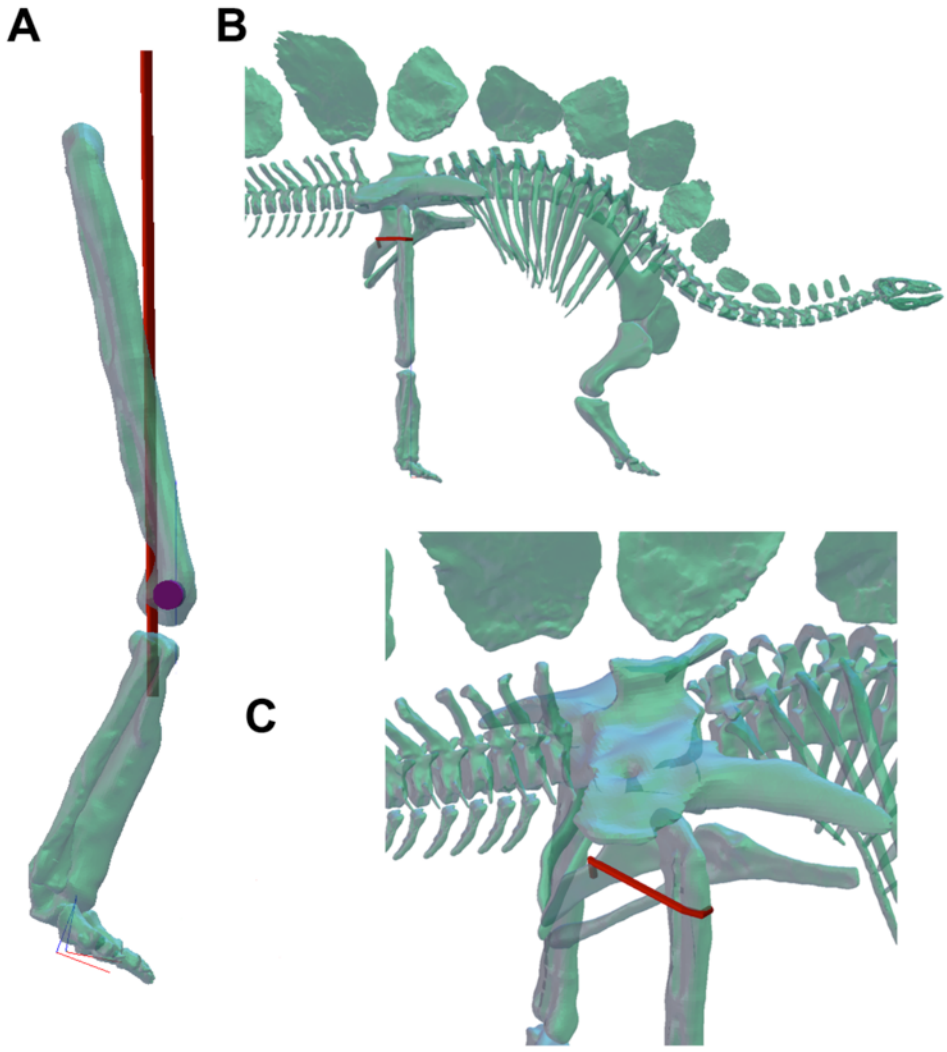

FIGURE 8. **A**, M. iliotibialis 1 intersects the surface of the femur when the knee is flexed if modeled as travelling in a straight line from origin to insertion; **B–C**, travel

path of M. ischiotrochantericus defined by a series of straight line segments separated by fixed via points. [Intended for column width].

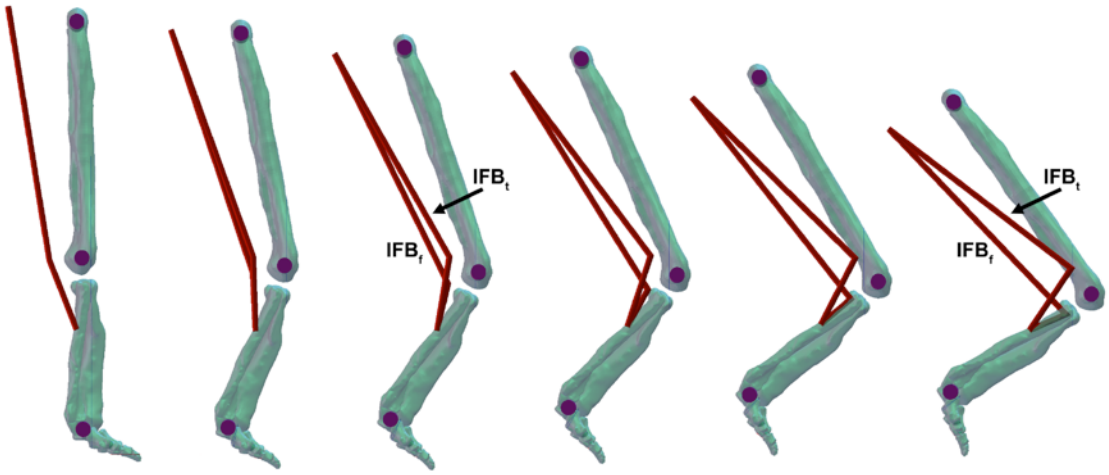

FIGURE 9. Muscle paths of the M. iliofibularis (IFB) from knee extension (left) to full flexion (right). $IFB_{f,}$ via point fixed relative to femur; $IFB_{t,}$ via point fixed relative to tibia. The path of IFB is strongly affected by the body segment to which the via point is fixed. Both muscle paths intersect the skeleton at high values for knee flexion, highlighting the importance of visually inspecting models throughout the entire limb range of motion. [Intended for page width].

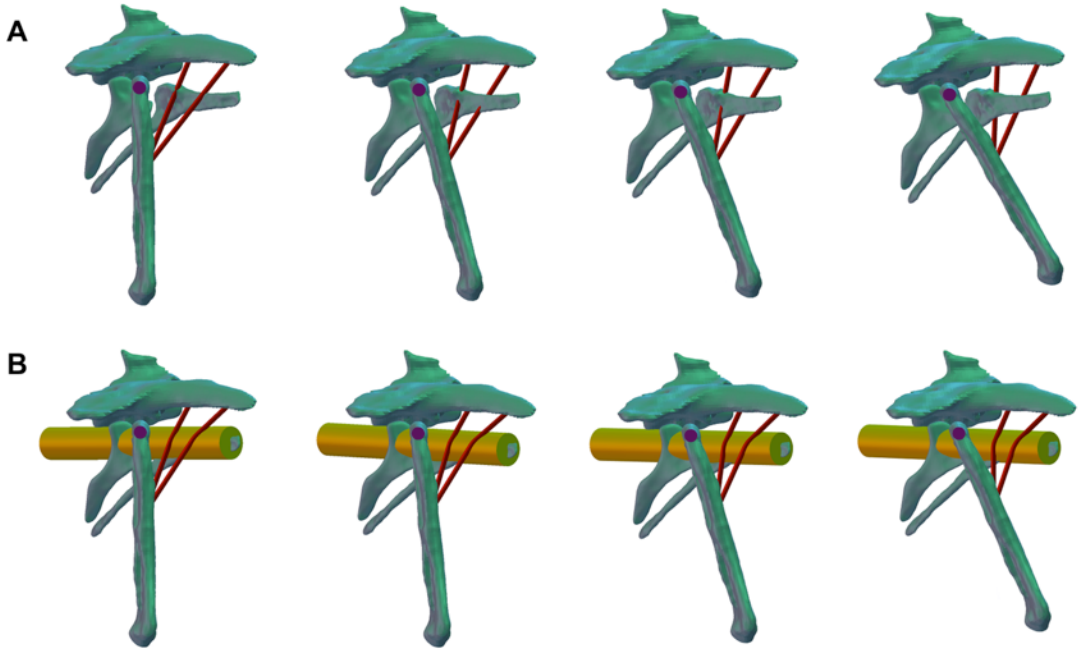

FIGURE 10. Muscle paths of the M. puboischiofemoralis internus (anterior and posterior) in *Stegosaurus stenops*. **A**, muscle paths intersect implausibly with the prepubis with increased femoral flexion when modelled as simple origin-insertion straight paths. **B**, muscle paths wrap around a cylinder positioned correspond to the surface contours of the prepubis, preventing intersection with the skeleton. [Intended for 2/3 page width].

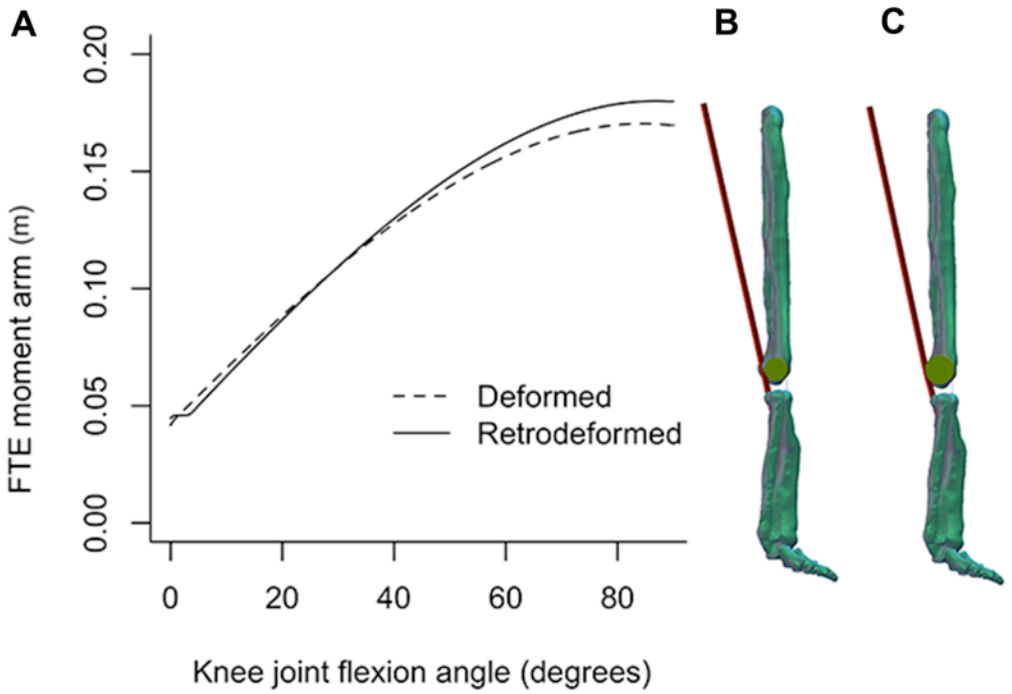

1954

1955 FIGURE 11. Calculation of moment arms for the M. flexor tibialis externus (FTE) in

1956 *Stegosaurus stenops*. **A**, variation in FTE moment arm with knee flexion. Positive

1957 values for moment arm indicate leverage for knee flexion. **B**, original model in which

1958 calculated joint center and cylinder radius is based upon deformed distal femoral

1959 condyles. **C**, modified model in which joint center and cylinder radius is altered to

1960 account for taphonomic damage, as outlined in Figure 7. [Intended for column width].

1961

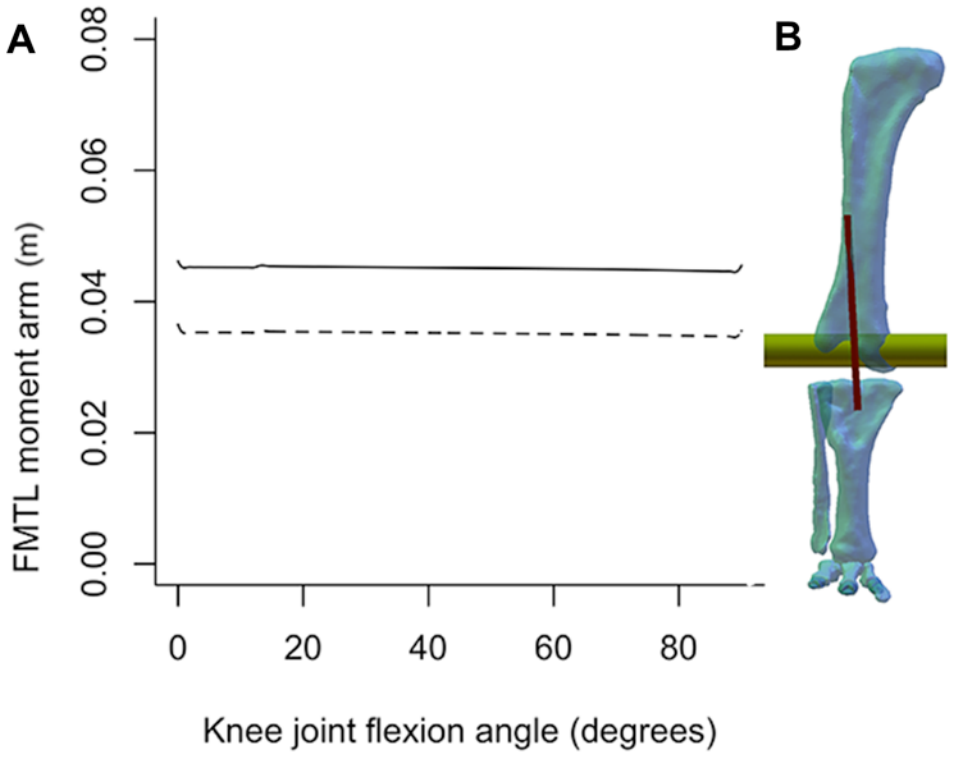

1962

1963 FIGURE 12. Calculation of M. femorotibialis lateralis (FMTL) moment arm in
1964 *Stegosaurus stenops.* Positive values for moment arm indicate leverage for knee
1965 extension. **A**, FMTL moment arm is constant throughout the entire range of motion of
1966 the knee; **B**, the path of FMTL is tightly constrained to wrap around the knee joint
1967 cylinder. Dashed line, moment arm around deformed condyles; solid line, moment
1968 arm calculated around retrodeformed condyles (as outlined in 'Joint Centers' section).
1969 [Intended for column width].

1970

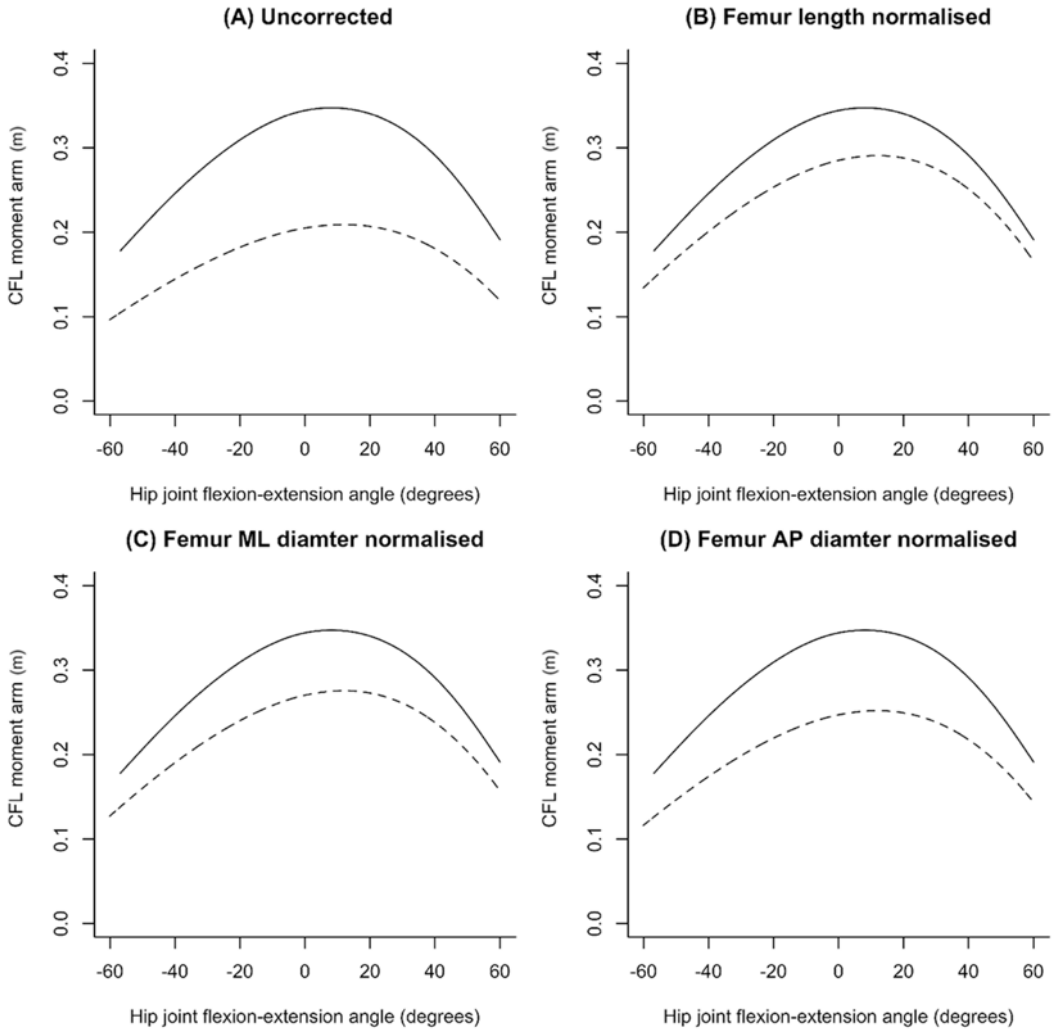

1971

1972 FIGURE 13. Moment arms calculated for M. caudofemoralis longus (CFL) around
1973 the hip in *Stegosaurus stenops* (solid line) and *Kentrosaurus aethiopicus* (dashed
1974 line). Positive values for moment arm indicate leverage for hip extension. **A**, moment
1975 arm values without normalization; **B**, moment arm normalized to femur length; **C**,
1976 moment arms normalized to mediolateral (ML) diameter; **D**, moment arm normalized
1977 to anteroposterior (AP) diameter. [Intended for 2/3 page width].